

Achievable information rates of ambient backscatter communications

Donatella Darsena, Giacinto Gelli, and Francesco Verde

Abstract

Ambient backscatter is an intriguing wireless communication paradigm that allows small devices to compute and communicate by using only the power they harvest from radio-frequency (RF) signals in the air. Ambient backscattering devices reflect existing RF signals emitted by legacy communications systems, such as digital TV broadcasting, cellular or Wi-Fi ones, which would be otherwise treated as harmful sources of interference. This paper deals with the ultimate performance limits of ambient backscatter systems in broadband fading environments, by considering different amounts of network state information at the receivers. After introducing a detailed signal model of the relevant communication links, we study the influence of physical parameters on the capacity of both legacy and backscatter systems. We find that, under reasonable operative conditions, a legacy system employing multicarrier modulation can turn the RF interference arising from the backscatter process into a form of multipath diversity that can be suitably exploited to noticeably increase its performance. Moreover, we show that, even when employing simple single-carrier modulation techniques, the backscatter system can achieve significant data rates over relatively short distances, especially when the intended recipient of the backscatter signal is co-located with the legacy transmitter, i.e., they are on the same machine.

Index Terms

Ambient backscatter, ergodic and outage capacity, symbol variance and amplitude constraints, multi-carrier systems, performance bounds.

I. INTRODUCTION

Electromagnetic (EM) interference, also called radio-frequency (RF) interference, has been traditionally treated as a disturbance in the design of wireless communications systems. However, RF signals carry information as well as energy at the same time. Such a dual nature of EM interference is stimulating a significant interest in communications systems powered by harvested ambient energy. In particular, *ambient backscatter* has emerged as a novel communication paradigm, where a small passive device can transmit its own data by backscattering the EM/RF wave deriving from existing or *legacy* communication systems, such as digital TV (DTV) broadcasting, cellular systems, or wireless local area networks (LANs), e.g., Wi-Fi. Unlike traditional backscatter systems, such as radio frequency identification (RFID) ones [1], [2], ambient backscatter does not require a dedicated reader, which allows for direct device-to-device (D2D) and even multi-hop communications. Recently, this new communication paradigm has been receiving much attention [3], [4], [5], [6], [7], [8], since it can be embedded into inexpensive objects in order to fulfil the ubiquitous and pervasive communication vision of the Internet-of-Things (IoT) [9].

D. Darsena is with the Department of Engineering, Parthenope University, Naples I-80143, Italy (e-mail: darsena@uniparthenope.it). G. Gelli and F. Verde are with the Department of Electrical Engineering and Information Technology, University Federico II, Naples I-80125, Italy [e-mail: (gelli,f.verde)@unina.it].

The main principles of ambient backscatter were first introduced in [3], where also a simple prototype is developed, which harvests DTV energy to achieve D2D communications with rates of 1 kbps over a range of about 8 m outdoor and 5 m indoor. In [4], the same principles are exploited to allow a passive device or *tag* to directly connect to the Internet by leveraging on an existing Wi-Fi infrastructure. In particular, in the scenario of [4], the tag can establish bidirectional communications with a Wi-Fi device by modulating the channel state information (CSI) or received signal strength indicator (RSSI) of the Wi-Fi channel (in the uplink) or by simple on-off modulation (in downlink), achieving rates of 0.5 kbps in uplink over a range of 1 m and up to 20 kbps over 2.2 m in downlink. A significant improvement over this scheme is the BackFi system proposed in [5], wherein backscatter communications can achieve at least 1 Mbps over a 5m-range in uplink, by exploiting the signal cancellation principles of full-duplex systems [10].

In [6], [7], [8] the ambient backscatter approach is extended to systems where the backscatter receiver (called the reader) is equipped with multiple antennas; moreover, a detailed analysis of the system from a signal processing perspective is carried out, by assuming that the wireless channel obeys a frequency-flat block-fading model. Since the tag employs low-rate differentially-encoded on-off signaling, the reader can decode its information by employing simple noncoherent detection strategies. The performance analysis of the approach proposed in [6], [7], [8] is carried out in terms of bit-error rate (BER), both analytically and by Monte Carlo simulations.

Existing research on ambient backscatter has covered both experimental and theoretical aspects. However, to the best of our knowledge, an investigation of the ultimate performance limits of ambient backscatter, in terms of information-theoretic figures, such as the ergodic or outage capacity, is still lacking. We aim at filling this gap, by evaluating in this paper the capacity (i.e., the maximum achievable transmission rate) of ambient backscatter communications systems. Our analysis assumes that the legacy system employs a multicarrier modulation, which is ubiquitous in modern communication systems, whereas the backscatter system transmits at lower bit-rates by adopting simple single-carrier techniques. We evaluate typical information-theoretic figures of merit for both the legacy and the backscatter systems, by assuming a symbol variance constraint for the legacy system and both symbol variance and amplitude constraints for the backscatter one. Our results allow one to assess the maximum data-rate achievable by the backscatter system, and also show somewhat surprisingly that, since the backscatter transmitter acts as a relay towards the legacy receiver, the legacy system can even benefit of ambient backscatter, provided that some reasonable assumptions are met. In other words, ambient backscatter is not only a viable means of opportunistically capitalizing on the energy carried out by RF signals, but it is also a way of turning EM interference into a form of diversity.

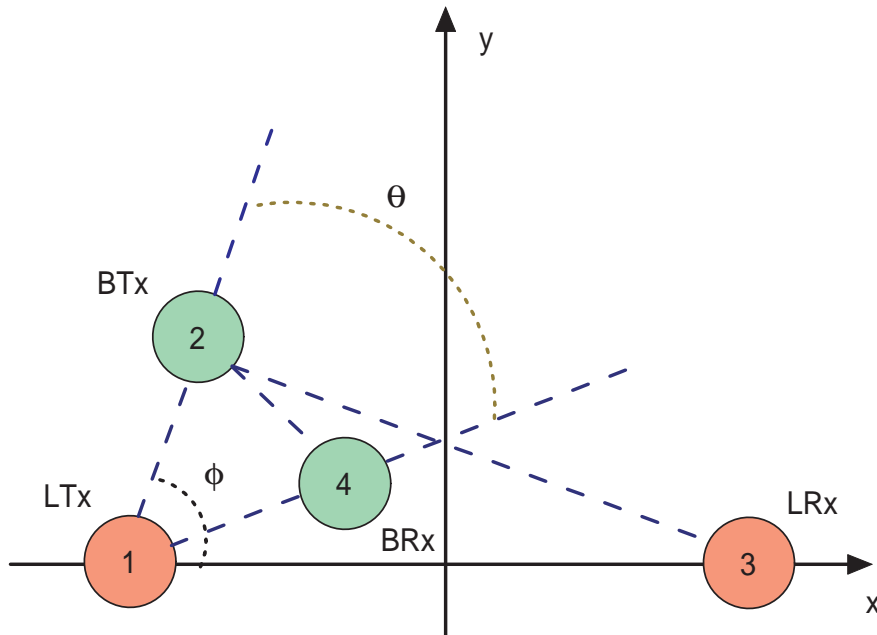


Figure 1. The considered wireless network model: in red, the legacy transmitting (node 1) and receiving (node 3) devices; in green, the backscatter transmitter (node 2) and its intended recipient (node 4).

The paper is organized as follows. The system model is introduced in Section II. General assumptions underlying the performance analysis are pointed out in Section III. The analytical performance analysis is carried out in Sections IV and V for the legacy and the backscatter system, respectively. Numerical results corroborating our analysis are reported in Section VI. Conclusions are drawn in Section VII.

II. AMBIENT BACKSCATTER SYSTEM MODEL

In this section, we introduce a model for ambient backscatter communications that harvest energy from legacy transmissions: our model builds on the previous works [3], [4], [5].

The considered wireless network is depicted in Fig. 1: it is composed of a *legacy*¹ transmitter-receiver (LTx/LRx) pair and a *backscatter* transmitter (BTx) that wishes to transmit information-bearing symbols to an intended recipient (BRx). In the sequel, the devices LTx, BTx, LRx, and BRx will be labelled as nodes 1, 2, 3, and 4, respectively. Specifically, the LTx and LRx are *active* devices, i.e., they have internal power sources to modulate and demodulate, respectively, the relevant RF signals. On the other hand, the BTx is a *passive* device, i.e., it does not include any active RF component, and communicates using only the power that it harvests from the RF signals transmitted by the LTx. Finally, the BRx may be either passive or might use typical active RF electronics to demodulate the signal backscattered by the BTx.

¹Hereinafter, similarly to [3], the term “legacy” refers to existing wireless communications technologies, such as, e.g., DTV, cellular, and Wi-Fi systems.

The LTx adopts a *multicarrier* modulation scheme with M subcarriers. The block of data to be transmitted by the LTx within the n th ($n \in \mathbb{Z}$) frame of length T_s is denoted as $\mathbf{s}(n) \triangleq [s^{(0)}(n), s^{(1)}(n), \dots, s^{(M-1)}(n)]^T \in \mathbb{C}^M$, whose entries are independent and identically distributed (i.i.d.) zero-mean circularly symmetric complex symbols, with variance $\sigma_s^2 \triangleq \mathbb{E}[|s^{(m)}(n)|^2]$, for any $m \in \mathcal{M} \triangleq \{0, 1, \dots, M-1\}$ and $n \in \mathbb{Z}$. The vector $\mathbf{s}(n)$ is subject to conventional multicarrier precoding, encompassing M -point inverse discrete Fourier transform (IDFT), followed by cyclic prefix (CP) insertion of length $L_{\text{cp}} < M$. It results that $T_s \triangleq P T_c$, with $P \triangleq M + L_{\text{cp}}$ and T_c denoting the sampling period of the legacy system. The data block transmitted by the LTx can be compactly expressed [12] as $\mathbf{u}(n) = \mathbf{T}_{\text{cp}} \mathbf{W}_{\text{IDFT}} \mathbf{s}(n)$, where $\mathbf{T}_{\text{cp}} \triangleq [\mathbf{I}_{\text{cp}}^T, \mathbf{I}_M]^T \in \mathbb{R}^{P \times M}$, with $\mathbf{I}_{\text{cp}} \in \mathbb{R}^{L_{\text{cp}} \times M}$ obtained from \mathbf{I}_M by picking its last L_{cp} rows, and $\mathbf{W}_{\text{IDFT}} \in \mathbb{C}^{M \times M}$ is the unitary symmetric IDFT matrix [12].² The entries of $\mathbf{u}(n)$ are subject to D/A plus RF conversion for transmission over the wireless channel.

On the other hand, due to its power limitation, the BTx transmits in a narrower bandwidth with respect to the legacy system (higher data rates consume more power and energy). Specifically, the BTx has a Q -order symbol sequence $\{b(n)\}_{n \in \mathbb{Z}} \in \mathcal{B} \triangleq \{\beta_1, \beta_2, \dots, \beta_Q\}$ of i.i.d. zero-mean circularly symmetric complex symbols destined for the BRx, with variance $\sigma_b^2 \triangleq \mathbb{E}[|b(n)|^2]$, for any $n \in \mathbb{Z}$, and signaling interval T_s . Such a sequence is arranged in consecutive frames of $B \in \mathbb{N}$ symbols, whose duration is less than or equal to the coherence time $T_{\text{coh}} \triangleq B T_s$ of the channels. It is noteworthy that one symbol is transmitted by the BTx per each frame of the legacy system.

A. Signal backscattered by the BTx

Since the BTx is passive, it cannot initiate transmissions on its own. Once the LTx transmits the block $\mathbf{u}(n)$, the EM wave propagates toward the BTx. When the wave reaches the BTx, its antenna is excited and the RF power is converted to direct current (DC) power through a *power harvester*. This DC voltage is then able to power the control logic on the chip, whose task is to modulate the reflected EM wave.

Regarding the $1 \rightarrow 2$ link, a frequency-selective and quasi-static channel model is assumed. Specifically, during an interval of duration T_{coh} , the channel impulse response spans $L_{12} \in \mathbb{N}$ sampling periods T_c ; hence, the resulting discrete-time channel $c_{12}(\ell)$ is a causal system of order L_{12} , i.e., $c_{12}(\ell) \equiv 0$ for $\ell \notin \{0, 1, \dots, L_{12}\}$. Moreover, the $1 \rightarrow 2$ link is characterized by the (integer) time offset (TO) $\theta_{12} \in \mathbb{N}$,

²Besides standard notations, we adopt the following ones: matrices [vectors] are denoted with upper [lower] case boldface letters (e.g., \mathbf{A} or \mathbf{a}); the superscripts $*$, T , H , and -1 denote the conjugate, the transpose, the conjugate transpose, and the inverse of a matrix, respectively; $\log(\cdot)$ is taken to the base 2; the operator $\mathbb{E}(\cdot)$ denotes ensemble averaging; $\mathbf{O}_{m \times n} \in \mathbb{R}^{m \times n}$ and $\mathbf{I}_m \in \mathbb{R}^{m \times m}$ denote the null and the identity matrices, respectively; matrix $\mathbf{A} = \text{diag}(a_0, a_1, \dots, a_{n-1})$ is diagonal; $\mathbf{F} \in \mathbb{R}^{n \times n}$ and $\mathbf{B} \in \mathbb{R}^{n \times n}$ denote the Toeplitz ‘‘forward shift’’ and ‘‘backward shift’’ matrices [11], respectively, where the first column of \mathbf{F} and the first row of \mathbf{B} are given by $[0, 1, 0, \dots, 0]^T$ and $[0, 1, 0, \dots, 0]$, respectively; a circular symmetric complex Gaussian random vector $\mathbf{x} \in \mathbb{C}^n$ with mean $\boldsymbol{\mu} \in \mathbb{C}^n$ and covariance matrix $\mathbf{K} \in \mathbb{C}^{n \times n}$ is denoted as $\mathbf{x} \sim \mathcal{CN}(\boldsymbol{\mu}, \mathbf{K})$.

modeling the fact that the BTx does not know where the multicarrier blocks of the legacy system start.³ Finally, since the BTx simply remodulates the carrier of the LTx, we assume in the sequel that the carrier frequency offset (CFO) is negligible.⁴ Under these assumptions and provided that $L_{12} + \theta_{12} \leq P - 1$,⁵ the baseband-equivalent block received by the BTx within the n th frame can be written as

$$\tilde{\mathbf{r}}_2(n) = \tilde{\mathbf{C}}_{12}^{(0)} \mathbf{u}(n) + \tilde{\mathbf{C}}_{12}^{(1)} \mathbf{u}(n - 1) \quad (1)$$

where $\tilde{\mathbf{r}}_2(n) \triangleq [r_2^{(0)}(n), r_2^{(1)}(n), \dots, r_2^{(P-1)}(n)]^T \in \mathbb{C}^P$,

$$\tilde{\mathbf{C}}_{12}^{(0)} \triangleq \sum_{\ell=0}^{L_{12}} c_{12}(\ell) \mathbf{F}^{\ell+\theta_{12}} \in \mathbb{C}^{P \times P} \quad (2)$$

$$\tilde{\mathbf{C}}_{12}^{(1)} \triangleq \sum_{\ell=0}^{L_{12}} c_{12}(\ell) \mathbf{B}^{P-\ell-\theta_{12}} \in \mathbb{C}^{P \times P} \quad (3)$$

are Toeplitz lower- and upper-triangular matrices, respectively, and we have neglected the noise introduced by the BTx [1], [13], since the latter employs only passive components and does not perform sophisticated signal processing operations. It is worth noticing that the last $P - L_{12} - \theta_{12}$ rows of the matrix $\tilde{\mathbf{C}}_{12}^{(1)}$ are identically zero, that is, the interblock interference (IBI) contribution is entirely contained in the first $L_{12} + \theta_{12}$ entries of the received vector $\tilde{\mathbf{r}}_2(n)$.

In our ambient backscatter framework, the BTx acts as a digital multilevel modulator, mapping each information symbol onto a set of Q waveforms by means of a proper variation of its chip impedance [14]. To elaborate upon this point, Fig. 2 reports the equivalent Thévenin circuit [15] of the BTx front-end, where the sine wave generator V_0 models the sinusoidal voltage induced by the power density of the incident EM field, $Z^a = R^a + jX^a \in \mathbb{C}$ is the antenna impedance, and $Z_q^c = R_q^c + jX_q^c \in \mathbb{C}$ are Q distinct values of the BTx chip impedance, for $q \in \mathcal{Q} \triangleq \{1, 2, \dots, Q\}$. The maximum power available from the generator is given by $\mathcal{P}_{\max}^c \triangleq |V_0|^2 / (8R^a)$.

At the reference plane denoted by the dashed line in Fig. 2, due to the impedance discontinuity, two power waves are generated: a (*nonreflecting*) *forward wave* propagating to the right and a (*reflecting*) *backward wave* giving rise to the backscattered field. When the switch S_q is closed, i.e., the chip impedance of the BTx takes on the value Z_q^c , the average power harvested by the BTx is given [16] by $\mathcal{P}_q^c = (1 - |\Gamma_q|^2) \mathcal{P}_{\max}^c$

³The fractional TO is incorporated as part of $\{c_{12}(\ell)\}_{\ell=0}^{L_{12}}$.

⁴A CFO may occur as a result of the Doppler effect from a mobile BTx, which is an unimportant phenomenon in backscatter systems [3], [4], [5].

⁵In general, the received block within the n th frame is affected not only by the IBI of the previous frame $n - 1$ but also by the IBI of the $(n - 2)$ th frame. The assumption $L_{ik} + \theta_{ik} \leq P - 1$ ensures that the sum of the TO and the channel order turns out to be within one frame, such that the n th received block is impaired only by the IBI of the previous frame.

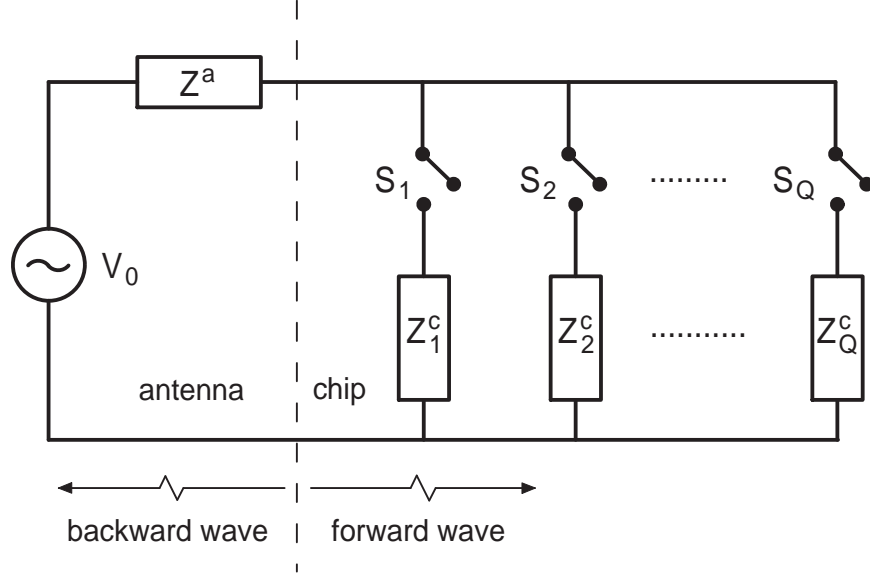


Figure 2. Equivalent Thévenin circuit of the multilevel backscatter transmitter.

($q \in \mathcal{Q}$), where⁶

$$\Gamma_q = \frac{(Z^a)^* - Z_q^c}{Z^a + Z_q^c} \quad (4)$$

is the *power wave reflection coefficient* $\Gamma_q \in \mathbb{C}$. The squared magnitude $0 \leq |\Gamma_q|^2 \leq 1$ of the power wave reflection coefficient is referred to as the *power reflection coefficient* [16]: it measures the fraction of \mathcal{P}_{\max}^c that is not delivered to the chip of the BTx. It is worth noticing that, if $(Z^a)^* = Z_q^c$ (*impedance matching condition*), then $\Gamma_q = 0$: in this case, the tag achieves maximum average power harvesting \mathcal{P}_{\max}^c and, in theory, there is no backscattered field. Hence, an impedance mismatch $(Z^a)^* \neq Z_q^c$ is necessary to reflect part of the energy from the BTx antenna back to the intended recipient BRx.

The symbol sequence $\{b(n)\}_{n \in \mathbb{Z}}$ can be embedded in the backscattered signal by carefully choosing the chip impedances $Z_1^c, Z_2^c, \dots, Z_Q^c$. Each chip impedance in Fig. 2 corresponds to a point of the symbol constellation \mathcal{B} . More precisely, to produce impedance values realizable with passive components, all the power wave reflection coefficients $\Gamma_1, \Gamma_2, \dots, \Gamma_Q$ are confined in the complex plane within a circle centered at the origin with radius smaller than or equal to one. These coefficients are then scaled by a constant $0 \leq \alpha \leq 1$ such that

$$\Gamma_q = \alpha \beta_q \quad (q \in \mathcal{Q}) \quad (5)$$

with $|\beta_q| \leq 1$. Eq. (5) establishes a one-to-one mapping between the information symbols of the BTx and the power wave reflection coefficients of its chip. Such a mapping is generally referred to as *backscatter*

⁶The power wave reflection coefficient Γ_q depends on the chip impedance that, in its turn, depends on the chip input power. A linearized model is herein assumed for the power wave reflection coefficient [17], according to which Γ_q does not depend on the incident power.

or *load modulation* [14]. The choice of α governs the harvesting-performance tradeoff of the backscatter communication process. Indeed, values of α closer to one allows the BTx to reflect increasing amounts of the incident field back to the BRx, resulting thus in greater backscatter signal strengths (i.e., for a target symbol error probability at the BRx, larger communication ranges). On the other hand, values of α much smaller than one allow a larger part of the incident field to be absorbed by the RF-to-DC conversion circuits of the BTx, hence improving power conversion (i.e., \mathcal{P}_q^c) at the expense of backscatter signal strength. We note that $\alpha = 0$ accounts for the case when the backscatter system is in sleep mode and, hence, only the legacy transmission is active.

Once α and \mathcal{B} have been chosen in accordance with certain criteria [1] and, thus, the power wave reflection coefficients are identified through (5), the chip impedances $Z_1^c, Z_2^c, \dots, Z_Q^c$ corresponding to the designed signal constellation can be obtained from (4) as follows

$$Z_q^c = \frac{(Z^a)^* - Z^a \Gamma_q}{1 + \Gamma_q} \quad (q \in \mathcal{Q}) \quad (6)$$

where Z^a is a given parameter. In practice, some constraints may be imposed on the chip impedances (6): for instance, to use high-quality electronic components and/or reduce the physical size of the BTx, it might be required to use resistors and capacitors, by hence eliminating inductors [14].

According to the antenna scatterer theorem [18], the EM field backscattered from the antenna of the BTx can be divided [18] into load-dependent (or *antenna mode*) scattering and load-independent (or *structural mode*) one: the former component can be associated with re-radiated power and depends on the chip impedances of the BTx, whereas the latter one can be interpreted as scattering from an open-circuited antenna. Therefore, with reference to antenna mode scattering and accounting for (5), the p th baseband-equivalent T_c -spaced sample backscattered by the BTx during the n th frame of the legacy system assumes the expression $x_2^{(p)}(n) = \Gamma(n) r_2^{(p)}(n)$ ($p \in \mathcal{P}$), where $\Gamma(n) \triangleq \alpha b(n)$ is a discrete random variable assuming the values $\Gamma_1, \Gamma_2, \dots, \Gamma_Q$, whereas $b(n) \in \mathcal{B}$ is the symbol transmitted by the BTx during the n th frame. The corresponding block model reads as

$$\tilde{\mathbf{x}}_2(n) = \Gamma(n) \tilde{\mathbf{r}}_2(n) = \alpha b(n) \tilde{\mathbf{r}}_2(n) \quad (7)$$

where $\tilde{\mathbf{x}}_2(n) \triangleq [x_2^{(0)}(n), x_2^{(1)}(n), \dots, x_2^{(P-1)}(n)]^T \in \mathbb{C}^P$ and $\tilde{\mathbf{r}}_2(n)$ is given by (1).

B. Signal received by the LRx

With reference to the $1 \rightarrow 3$ and $2 \rightarrow 3$ links, we maintain the same assumptions previously made for the $1 \rightarrow 2$ link: basically, for $i \in \{1, 2\}$, within the coherence time T_{coh} , the resulting discrete-time channel $c_{i3}(\ell)$ is a causal system of order L_{i3} , i.e., $c_{i3}(\ell) \equiv 0$ for $\ell \notin \{0, 1, \dots, L_{i3}\}$, and $\theta_{i3} \in \mathbb{N}$ is the

corresponding TO. Since the BTx reflects the RF signal transmitted by the LTx, both $1 \rightarrow 3$ and $2 \rightarrow 3$ transmissions occur at the same RF frequency. For such a reason, we assume that the corresponding CFOs are equal and can be accurately estimated and compensated at the LRx through conventional techniques [19].

Provided that $L_{13} + \theta_{13} \leq P - 1$ and $L_{23} + \theta_{23} \leq P - 1$ (see footnote 5), accounting for (1) and (7), after CFO compensation, the baseband-equivalent vector received by the LRx within the n th frame of the legacy system can be expressed as

$$\begin{aligned} \tilde{\mathbf{r}}_3(n) &= \tilde{\mathbf{C}}_{13}^{(0)} \mathbf{u}(n) + \tilde{\mathbf{C}}_{13}^{(1)} \mathbf{u}(n-1) + \tilde{\mathbf{C}}_{23}^{(0)} \tilde{\mathbf{x}}_2(n) + \tilde{\mathbf{C}}_{23}^{(1)} \tilde{\mathbf{x}}_2(n-1) + \tilde{\mathbf{v}}_3(n) \\ &= \left[\tilde{\mathbf{C}}_{13}^{(0)} + \alpha b(n) \tilde{\mathbf{C}}_{23}^{(0)} \tilde{\mathbf{C}}_{12}^{(0)} \right] \mathbf{u}(n) + \left[\tilde{\mathbf{C}}_{13}^{(1)} + \alpha b(n) \tilde{\mathbf{C}}_{23}^{(0)} \tilde{\mathbf{C}}_{12}^{(1)} + \alpha b(n-1) \tilde{\mathbf{C}}_{23}^{(1)} \tilde{\mathbf{C}}_{12}^{(0)} \right] \mathbf{u}(n-1) + \tilde{\mathbf{v}}_3(n) \end{aligned} \quad (8)$$

where $\{\tilde{\mathbf{C}}_{13}^{(0)}, \tilde{\mathbf{C}}_{13}^{(1)}\}$ and $\{\tilde{\mathbf{C}}_{23}^{(0)}, \tilde{\mathbf{C}}_{23}^{(1)}\}$ can be obtained from (2) and (3) by replacing $\{L_{12}, c_{12}(\ell), \theta_{12}\}$ with $\{L_{13}, c_{13}(\ell), \theta_{13}\}$ and $\{L_{23}, c_{23}(\ell), \theta_{23}\}$, respectively, and $\tilde{\mathbf{v}}_3(n) \in \mathbb{C}^P$ accounts for the structural mode scattering, which is independent of the BTx chip impedances, as well as for thermal noise. We have also observed that $\tilde{\mathbf{C}}_{23}^{(1)} \tilde{\mathbf{C}}_{12}^{(1)} = \mathbf{O}_{P \times P}$, under the assumption that

$$L_{12} + L_{23} + \theta_{12} + \theta_{23} \leq P - 1. \quad (9)$$

The set of lower (upper) triangular Toeplitz matrices possesses an eminent algebraic structure: indeed, such a set is an *algebra* [11]. In particular, the product of any lower (upper) triangular Toeplitz matrices is a lower (upper) triangular Toeplitz matrix, too. Indeed, it is directly verified that, if (9) holds, the product $\tilde{\mathbf{C}}_{23}^{(0)} \tilde{\mathbf{C}}_{12}^{(0)}$ is a lower-triangular Toeplitz matrix having as first column $[\mathbf{0}_{\theta_{12}+\theta_{23}}^T, \mathbf{c}_{123}^T(n), \mathbf{0}_{P-L_{12}-L_{23}-\theta_{12}-\theta_{23}-1}^T]^T$, where the vector $\mathbf{c}_{123} \in \mathbb{C}^{L_{12}+L_{23}+1}$ collects the samples of the (linear) convolution between $\{c_{12}(\ell)\}_{\ell=0}^{L_{12}}$ and $\{c_{23}(\ell)\}_{\ell=0}^{L_{23}}$. Under the assumption that

$$L_{\text{cp}} \geq \max(L_{13} + \theta_{13}, L_{12} + L_{23} + \theta_{12} + \theta_{23}) \quad (10)$$

the IBI contribution in (8) can be completely discarded by dropping the first L_{cp} components of $\tilde{\mathbf{r}}_3(n)$, since it is verified by direct inspection that: (i) only the first $L_{12} + L_{23} + \theta_{12} + \theta_{23}$ rows of $\tilde{\mathbf{C}}_{23}^{(0)} \tilde{\mathbf{C}}_{12}^{(0)}$ are possibly nonzero; (ii) the last $P - L_{23} - \theta_{23}$ rows of the matrix $\tilde{\mathbf{C}}_{23}^{(1)}$ are identically zero and, hence, the nonzero entries of $\tilde{\mathbf{C}}_{23}^{(1)} \tilde{\mathbf{C}}_{12}^{(0)}$ are located within its first $L_{23} + \theta_{23}$ rows; (iii) the last $P - L_{13} - \theta_{13}$ rows of $\tilde{\mathbf{C}}_{13}^{(1)}$ are identically zero. Therefore, if (10) is fulfilled, after discarding the CP, performing M -point discrete Fourier transform (DFT), the resulting frequency-domain data block $\mathbf{r}_3(n) \in \mathbb{C}^M$ is given by

$$\mathbf{r}_3(n) = \mathbf{\Psi}_3 \mathbf{s}(n) + \mathbf{v}_3(n) \quad (11)$$

where $\Psi_3 \triangleq \text{diag}[\Psi_3(0), \Psi_3(1), \dots, \Psi_3(M-1)]$, whose diagonal entries are given by

$$\Psi_3(m) \triangleq \Psi_{13}(m) + \alpha b(n) \Psi_{12}(m) \Psi_{23}(m) \quad (12)$$

for $m \in \mathcal{M}$, with

$$\Psi_{ik}(m) \triangleq e^{-j\frac{2\pi}{M}\theta_{ik}m} \sum_{\ell=0}^{L_{ik}} c_{ik}(\ell) e^{-j\frac{2\pi}{M}\ell m} \quad (13)$$

and $\mathbf{v}_3(n) \in \mathbb{C}^M$ is obtained from $\tilde{\mathbf{v}}_3(n)$ by discarding its first L_{cp} entries and performing M -point DFT.

Remark 1: It is noteworthy from (8)-(11) that the signal backscattered by the BTx may create additional paths from the LTx to the LRx, which increases multipath propagation on the legacy channel. In particular, if $L_{12} + L_{23} + \theta_{12} + \theta_{23} > L_{13} + \theta_{13}$, in accordance with (10), such an additional multipath requires a corresponding increase of the CP length in order to avoid both IBI and intercarrier interference (ICI) after CP removal, which may worsen the performance of the legacy system. In summary, the price to pay for allowing ambient backscatter is an oversizing of the CP length, thus leading to an inherent reduction of the transmission data rate of the legacy system. However, such a loss turns out to be negligible if the number M of subcarriers is significantly greater than L_{cp} . Most important, we show in Section IV that, if the legacy system is designed to fulfil (10), it might *even* achieve a performance gain.

Remark 2: We note that assumption (10) requires only upper bounds (rather than the exact knowledge) on the channel orders and TOs. This is a reasonable assumption in the considered scenario. Indeed, in general, depending on the transmitted signal parameters (carrier frequency and bandwidth) and environment (indoor or outdoor), the maximum channel multipath spread is known. For legacy systems, particular synchronization policies are typically adopted to drastically reduce the asynchronisms [20], whereas, for ambient backscatter communications, the distances among the LTx, BTx, and the BRx are very small. Therefore, the TOs are confined to a small uncertainty interval, whose support can be typically predicted.

C. Signal received by the BRx

Concerning the $1 \rightarrow 4$ and $2 \rightarrow 4$ links, we maintain the same assumptions previously made for the $1 \rightarrow 2$, $1 \rightarrow 3$, and $2 \rightarrow 3$ links: in summary, for $i \in \{1, 2\}$, within the coherence time T_{coh} , the resulting discrete-time channel $c_{i4}(\ell)$ is a causal system of order L_{i4} , i.e., $c_{i4}(\ell) \equiv 0$ for $\ell \notin \{0, 1, \dots, L_{i4}\}$, and $\theta_{i4} \in \mathbb{N}$ is the corresponding TO. Similarly to Subsection II-B, we assume that the $1 \rightarrow 4$ and $2 \rightarrow 4$ links have the same CFO, which will be denoted as $\nu \in (-1/2, 1/2)$ in the sequel (it is normalized to the subcarrier spacing $1/T_c$).

Under the assumption that $L_{14} + \theta_{14} \leq P - 1$ and $L_{24} + \theta_{24} \leq P - 1$ (see footnote 5), the baseband-equivalent block received by the BRx within the n th frame of the legacy system can be expressed as shown

$$\begin{aligned}
\tilde{\mathbf{r}}_4(n) &= e^{j\frac{2\pi}{M}\nu nP} \boldsymbol{\Sigma}_\nu \left[\tilde{\mathbf{C}}_{14}^{(0)} \mathbf{u}(n) + \tilde{\mathbf{C}}_{14}^{(1)} \mathbf{u}(n-1) + \tilde{\mathbf{C}}_{24}^{(0)} \tilde{\mathbf{x}}_2(n) + \tilde{\mathbf{C}}_{24}^{(1)} \tilde{\mathbf{x}}_2(n-1) \right] + \tilde{\mathbf{v}}_4(n) \\
&= \alpha e^{j\frac{2\pi}{M}\nu nP} \boldsymbol{\Sigma}_\nu \left[\tilde{\mathbf{C}}_{24}^{(0)} \tilde{\mathbf{C}}_{12}^{(0)} \mathbf{u}(n) + \tilde{\mathbf{C}}_{24}^{(0)} \tilde{\mathbf{C}}_{12}^{(1)} \mathbf{u}(n-1) \right] b(n) \\
&\quad + \alpha e^{j\frac{2\pi}{M}\nu nP} \boldsymbol{\Sigma}_\nu \tilde{\mathbf{C}}_{24}^{(1)} \tilde{\mathbf{C}}_{12}^{(0)} \mathbf{u}(n-1) b(n-1) \\
&\quad + e^{j\frac{2\pi}{M}\nu nP} \boldsymbol{\Sigma}_\nu \left[\tilde{\mathbf{C}}_{14}^{(0)} \mathbf{u}(n) + \tilde{\mathbf{C}}_{14}^{(1)} \mathbf{u}(n-1) \right] + \tilde{\mathbf{v}}_4(n) \quad (14)
\end{aligned}$$

at the top of this page in (14), where $\{\tilde{\mathbf{C}}_{14}^{(0)}, \tilde{\mathbf{C}}_{14}^{(1)}\}$ and $\{\tilde{\mathbf{C}}_{24}^{(0)}, \tilde{\mathbf{C}}_{24}^{(1)}\}$ can be obtained from (2) and (3) by replacing $\{L_{12}, c_{12}(\ell), \theta_{12}\}$ with $\{L_{14}, c_{14}(\ell), \theta_{14}\}$ and $\{L_{24}, c_{24}(\ell), \theta_{24}\}$, respectively, we have defined the diagonal matrix $\boldsymbol{\Sigma}_\nu \triangleq \text{diag}[1, e^{j\frac{2\pi}{M}\nu}, \dots, e^{j\frac{2\pi}{M}\nu(P-1)}] \in \mathbb{C}^{P \times P}$, and $\tilde{\mathbf{v}}_4(n) \mathbb{C}^P$ accounts for both the structural mode scattering and thermal noise.

Remark 3: It is important to notice from (14) that the BRx experiences *frequency-selective fast fading*, since: (i) the received signal is corrupted by the intersymbol interference (ISI) of the previous symbol $b(n-1)$; (ii) the channel tap seen by the BRx varies with time from sampling period to sampling period, due to its dependence on the data $\{u^{(p)}(n)\}_{p=0}^{P-1}$ transmitted by the LTx, and such a variation is P -times faster than the symbol rate $1/T_s$ of the backscatter system.

Interestingly, by observing that the nonzero entries of $\boldsymbol{\Sigma}_\nu \tilde{\mathbf{C}}_{24}^{(1)} \tilde{\mathbf{C}}_{12}^{(0)}$ are located within its first $L_{24} + \theta_{24}$ rows and the last $P - L_{14} - \theta_{14}$ rows of $\boldsymbol{\Sigma}_\nu \tilde{\mathbf{C}}_{14}^{(1)}$ are identically zero, the BRx can resort to a simple detection technique to completely remove its own ISI and partially mitigate the interference generated by the legacy transmission. More specifically, this can be obtained by dropping the first

$$L_b \geq \max(L_{14} + \theta_{14}, L_{24} + \theta_{24}) \quad (15)$$

components of $\tilde{\mathbf{r}}_4(n)$. This operation is accomplished by defining the matrix $\mathbf{R}_b \triangleq [\mathbf{O}_{N \times L_b}, \mathbf{I}_N] \in \mathbb{R}^{N \times P}$, with $N \triangleq P - L_b > 0$, and forming at the receiver the product $\mathbf{R}_b \tilde{\mathbf{r}}_4(n)$. So doing, one has

$$\mathbf{R}_b \tilde{\mathbf{r}}_4(n) = \alpha \mathbf{c}_4 b(n) + \mathbf{d}_4(n) \quad (16)$$

with

$$\mathbf{c}_4 \triangleq e^{j\frac{2\pi}{M}\nu nP} \mathbf{R}_b \boldsymbol{\Sigma}_\nu \left[\tilde{\mathbf{C}}_{24}^{(0)} \tilde{\mathbf{C}}_{12}^{(0)} \mathbf{u}(n) + \tilde{\mathbf{C}}_{24}^{(0)} \tilde{\mathbf{C}}_{12}^{(1)} \mathbf{u}(n-1) \right] \in \mathbb{C}^N \quad (17)$$

$$\mathbf{d}_4(n) \triangleq e^{j\frac{2\pi}{M}\nu nP} \mathbf{R}_b \boldsymbol{\Sigma}_\nu \tilde{\mathbf{C}}_{14}^{(0)} \mathbf{u}(n) + \mathbf{R}_b \tilde{\mathbf{v}}_4(n) \in \mathbb{C}^N \quad (18)$$

where it results that $\mathbf{R}_b \boldsymbol{\Sigma}_\nu \tilde{\mathbf{C}}_{24}^{(1)} \tilde{\mathbf{C}}_{12}^{(0)} = \mathbf{O}_{N \times P}$ and $\mathbf{R}_b \boldsymbol{\Sigma}_\nu \tilde{\mathbf{C}}_{14}^{(1)} = \mathbf{O}_{N \times P}$. To fulfil (15), some *a priori* knowledge is required at the BRx, which can be acquired in practice (see Remark 2): as explained in

Section V, such a knowledge at the BRx depend on whether the BRx and LTx are spatially-separated nodes [3] or they are the co-located [4], [5], i.e., they are on the same machine.

III. GENERAL ASSUMPTIONS FOR THE ANALYTICAL PERFORMANCE ANALYSIS

The goal of the forthcoming Sections IV and V is twofold. First, we aim at showing in Section IV what is the influence of the backscatter communication on the achievable rates of the legacy system, by assuming that the CP is long enough, i.e., inequality (10) is fulfilled. Second, under assumption (15), we highlight in Section V what are the ultimate rates of the backscatter communication, by considering either the case when the nodes BRx and LTx are co-located [4], [5] or the situation in which they are spatially-separated nodes [3]. General assumptions are reported in the sequel.

For $i \in \{1, 2\}$ and $k \in \{2, 3, 4\}$, with $i \neq k$, the channel samples $c_{ik}(0), c_{ik}(1), \dots, c_{ik}(L_{ik})$ (encompassing the physical channel as well as the transmit/receive filters) are modeled as i.i.d. zero-mean circularly symmetric complex Gaussian random coefficients (*Rayleigh fading model*),⁷ which are constant within the coherence time T_{coh} , but are allowed to vary independently in different coherence intervals; the variance $\mathbb{E}[|c_{ik}(\ell)|^2] \triangleq \sigma_{ik}^2 / (L_{ik} + 1)$ of the $i \rightarrow k$ link depends on the corresponding average path loss. Fading coefficients of different links are statistically independent among themselves, i.e., $c_{i_1 k_1}(\ell)$ is statistically independent of $c_{i_2 k_2}(\ell)$ for $i_1 \neq i_2$ or $k_1 \neq k_2$.

Since $c_{ik}(\ell)$ is a circularly symmetric complex Gaussian random variable by assumption, then $c_{ik}(\ell)$ and $c_{ik}(\ell) e^{-j\frac{2\pi}{M}(\ell + \theta_{ik})m}$ have the same probability distribution [21], i.e., $c_{ik}(\ell) e^{-j\frac{2\pi}{M}(\ell + \theta_{ik})m} \sim \mathcal{CN}[0, \sigma_{ik}^2 / (L_{ik} + 1)]$, for any ℓ, m , and n . Consequently, one has $\Psi_{ik}(m) \sim \mathcal{CN}(0, \sigma_{ik}^2)$. It is seen from (13) that, even if the time-domain channel taps $\{c_{ik}(\ell)\}_{\ell=0}^{L_{ik}}$ are assumed to be uncorrelated, the corresponding DFT samples $\Psi_{ik}(m_1)$ and $\Psi_{ik}(m_2)$ turn out to be correlated, for $m_1 \neq m_2 \in \mathcal{M}$. For $k \in \{3, 4\}$, we assume that $\tilde{\mathbf{v}}_k(n) \sim \mathcal{CN}(\mathbf{0}_P, \sigma_{v_k}^2 \mathbf{I}_P)$ with $\mathbb{E}[\tilde{\mathbf{v}}_k(n_1) \tilde{\mathbf{v}}_k^H(n_2)] = \mathbf{0}_{P \times P}$, for $n_1 \neq n_2 \in \mathbb{Z}$.

Finally, channel coefficients, information-bearing symbols, and noise samples are all modeled as statistically independent random variables.

IV. CAPACITY ANALYSIS OF THE LEGACY SYSTEM

Since the detection process at the LRx is carried out on a frame-by-frame basis, we omit the dependence on the frame index n hereinafter. Under the assumption that the realization Ξ_3 of Ψ_3 is known at the LRx (but not at the LTx), the channel output of (11) is the pair (\mathbf{r}_3, Ψ_3) . Therefore, the (*coherent*) *ergodic* (or

⁷Although the transmit/receive filters might introduce statistical correlation among channel taps, it is a common practice [20] to neglect such a correlation when evaluating the performance of multicarrier systems.

Shannon) capacity of (11) is defined as (see, e.g., [22])

$$C_3 \triangleq \sup_{f(\mathbf{s}) \in \mathcal{I}_s} \frac{I(\mathbf{s}; \mathbf{r}_3, \Psi_3)}{M} \quad (\text{in b/s/Hz}) \quad (19)$$

where $f(\mathbf{s})$ is the probability density function (pdf) of \mathbf{s} , \mathcal{I}_s is the set of admissible input distributions having the variance constraint $\mathbb{E}(\|\mathbf{s}\|^2) = M\sigma_s^2$ and $I(\mathbf{s}; \mathbf{r}_3, \Psi_3)$ denotes the mutual information [23], [24] between \mathbf{s} and (\mathbf{r}_3, Ψ_3) . The ergodic capacity can be achieved if the length of the codebook is long enough to reflect the ergodic nature of fading [25] (i.e., the duration of each transmitted codeword is much greater than the channel coherence time).

By using the chain rule for mutual information [23], [24] and observing that \mathbf{s} and Ψ_3 are statistically independent, it results that $I(\mathbf{s}; \mathbf{r}_3, \Psi_3) = I(\mathbf{s}; \Psi_3) + I(\mathbf{s}; \mathbf{r}_3 | \Psi_3) = I(\mathbf{s}; \mathbf{r}_3 | \Psi_3) = \mathbb{E}_{\Psi_3}[I(\mathbf{s}; \mathbf{r}_3 | \Psi_3 = \Xi_3)]$, where $I(\mathbf{s}; \mathbf{r}_3 | \Psi_3)$ is the mutual information between \mathbf{s} and \mathbf{r}_3 , given Ψ_3 . It is shown in [22] that, given $\Psi_3 = \Xi_3$, the input distribution that maximizes $I(\mathbf{s}; \mathbf{r}_3 | \Psi_3 = \Xi_3)$ is $\mathbf{s} \sim \mathcal{CN}(\mathbf{0}_M, \sigma_s^2 \mathbf{I}_M)$ and the corresponding maximal mutual information $I_{\max}(\mathbf{s}; \mathbf{r}_3 | \Psi_3 = \Xi_3)$ is given by

$$I_{\max}(\mathbf{s}; \mathbf{r}_3 | \Psi_3 = \Xi_3) = \log \det \left(\mathbf{I}_M + \frac{\sigma_s^2}{\sigma_{v_3}^2} \Xi_3 \Xi_3^H \right). \quad (20)$$

Consequently, one has

$$C_3 = \frac{1}{M} \mathbb{E} \left[\log \det \left(\mathbf{I}_M + \frac{\sigma_s^2}{\sigma_{v_3}^2} \Psi_3 \Psi_3^H \right) \right] = \frac{1}{M} \sum_{m=0}^{M-1} \mathbb{E} \left[\log \left(1 + \frac{\sigma_s^2}{\sigma_{v_3}^2} |\Psi_3(m)|^2 \right) \right] \quad (21)$$

where $\Psi_3(m)$ has been defined in (12).

A first step towards the analytical computation of C_3 consists of observing that, conditioned on the product $b\Psi_{12}(m)$, $|\Psi_3(m)|^2$ turns out to be exponentially distributed with mean $\sigma_{13}^2 + \alpha^2 \sigma_{23}^2 |b|^2 |\Psi_{12}(m)|^2$ ($m \in \mathcal{M}$). Thus, by applying the conditional expectation rule [31], one obtains

$$C_3 = -\frac{\log e}{M} \sum_{m=0}^{M-1} \mathbb{E} \left\{ e^{1/\Upsilon_3(m)} \text{Ei}[-1/\Upsilon_3(m)] \right\} \quad (22)$$

where $\text{Ei}(x) \triangleq \int_{-\infty}^x e^u/u \, du$ denotes the exponential integral function, for $x < 0$, and

$$\Upsilon_3(m) \triangleq \Gamma_{13} \left[1 + \alpha^2 \frac{\sigma_{23}^2}{\sigma_{13}^2} |b|^2 |\Psi_{12}(m)|^2 \right] \quad (23)$$

with $\Gamma_{13} \triangleq (\sigma_{13}^2 \sigma_s^2)/\sigma_{v_3}^2$ representing the average signal-to-noise ratio (SNR) over the $1 \rightarrow 3$ link. When the backscatter system is inactive, i.e., $\alpha = 0$, in accordance with [26], the ergodic capacity of the legacy system is given by

$$C_3|_{\alpha=0} = -e^{1/\Gamma_{13}} \text{Ei}(-1/\Gamma_{13}) \log e. \quad (24)$$

A first result can be obtained by comparing (22) and (24). Indeed, since $\Upsilon_3(m) \geq \Gamma_{13}$ for any realizations of $|b|^2$ and $|\Psi_{12}(m)|^2$ and, moreover, $-e^{1/x} \text{Ei}(-1/x)$ is a monotonically increasing function of $x \geq 0$, it follows that $C_3 \geq C_3|_{\alpha=0}$.

Remark 4: If the constraint (10) on the CP length is satisfied, then backscatter communications can even increase the ergodic capacity of the legacy system. Strictly speaking, the interference generated by the backscatter communication is turned into a form of diversity for the legacy system.

To assess the performance gain $\Delta C_3 \triangleq C_3 - C_3|_{\alpha=0}$, we use asymptotic expressions for C_3 by considering both low- and high-SNR regimes. With this goal in mind, we assume that $\sigma_{ik}^2 = d_{ik}^{-\eta}$, where d_{ik} is the distance between nodes i and k , and η denotes the path-loss exponent. Specifically, since $-e^{1/x} \text{Ei}(-1/x) \rightarrow x$ as $x \rightarrow 0$ [26], in the low-SNR regime, i.e., $\text{SNR}_L \triangleq \sigma_s^2/\sigma_{v_3}^2 \rightarrow 0$, one has

$$C_3|_{\alpha=0} \rightarrow \Gamma_{13} \log e \quad (25)$$

and

$$C_3 \rightarrow \frac{\log e}{M} \sum_{m=0}^{M-1} \mathbb{E}[\Upsilon_3(m)] = \Gamma_{13} \left[1 + \alpha^2 \sigma_b^2 \frac{\sigma_{12}^2 \sigma_{23}^2}{\sigma_{13}^2} \right] \log e, \quad \text{for } \text{SNR}_L \rightarrow 0 \quad (26)$$

which leads to

$$\Delta C_3 \rightarrow \alpha^2 \sigma_b^2 \frac{\sigma_s^2}{\sigma_{v_3}^2} \left(\frac{1}{d_{12} d_{23}} \right)^\eta \log e, \quad \text{for } \text{SNR}_L \rightarrow 0. \quad (27)$$

where, according to (5), it results that $\sigma_b^2 = \mathbb{E}(|b|^2) \leq 1$.

On the other hand, by using the fact that $-e^{1/x} \text{Ei}(-1/x) \rightarrow \log(1+x) - \gamma$ as $x \rightarrow +\infty$ [26], where $\gamma \triangleq \lim_{i \rightarrow \infty} \left[i^{-1} \sum_{k=1}^i k^{-1} - \log(i) \right] \approx 0.57721$ is the Euler-Mascheroni constant, we have that, in the high-SNR regime, i.e., when $\text{SNR}_L \rightarrow +\infty$,

$$C_3|_{\alpha=0} \rightarrow [\log(1 + \Gamma_{13}) - \gamma] \log e \quad (28)$$

and, moreover,

$$C_3 \rightarrow \frac{\log e}{M} \sum_{m=0}^{M-1} \mathbb{E}\{\log[1 + \Upsilon_3(m)] - \gamma\}, \quad \text{for } \text{SNR}_L \rightarrow +\infty. \quad (29)$$

To analytically compute the ensemble average in (29), we assume that the backscatter system employs a constant-modulus constellation, e.g., Q -ary phase-shift keying (PSK), with average energy $\sigma_b^2 = 1$. Henceforth, $|b| = 1$ and, by observing that $|\Psi_{12}(m)|^2$ is exponentially distributed with mean σ_{12}^2 , after some calculations, one has

$$\Delta C_3 \rightarrow -e^{1/\Omega_3} \text{Ei}(-1/\Omega_3) \log^2 e, \quad \text{for } \text{SNR}_L \rightarrow +\infty \quad (30)$$

with

$$\Omega_3 \triangleq \alpha^2 \frac{\sigma_{23}^2 \sigma_{12}^2}{\sigma_{13}^2} = \alpha^2 \left(\frac{d_{13}}{d_{12} d_{23}} \right)^\eta \quad (31)$$

where we observed that $\Gamma_{13}/(1 + \Gamma_{13}) \rightarrow 1$ as $\text{SNR}_L \rightarrow +\infty$. Two remarks are now in order.

Remark 5: The capacity gain ΔC_3 increases with α^2 , that is, the greater the backscatter signal strength, the greater the capacity gain of the legacy system. Such a result directly comes from the fact that the backscatter device can be regarded as a non-regenerative relay for the legacy system.

Remark 6: With reference to Fig. 1, let the angle ϕ between nodes 2 and 3 and the distance d_{13} between the LTx and the LRx be fixed. As a consequence of the Carnot's cosine law $d_{23} = (d_{12}^2 + d_{13}^2 - 2 d_{12} d_{13} \cos \phi)^{1/2}$, which can be substituted in (27) and (31). By using standard calculus concepts, it can be verified that, in both low- and high-SNR regimes, ΔC_3 is *not* a monotonic function of the distance d_{12} between the LTx and the BTx, for each $\phi \in [0, 2\pi)$. Indeed, it results that ΔC_3 is a strictly decreasing function of d_{12}/d_{13} when $9 \cos^2 \phi - 8 < 0$, i.e., the angle ϕ belongs to the set

$$\mathcal{A} \triangleq \left\{ \arccos(2\sqrt{2}/3) < a < \pi - \arccos(2\sqrt{2}/3) \text{ and } \pi + \arccos(2\sqrt{2}/3) < a < 2\pi - \arccos(2\sqrt{2}/3) \right\} \quad (32)$$

i.e., the capacity gain decreases as the BTx moves away from the LTx. On the other hand, when $9 \cos^2 \phi - 8 \geq 0$, i.e., $\phi \notin \mathcal{A}$, the capacity ΔC_3 monotonically increases for $d_{\min}(\phi) \leq d_{12}/d_{13} \leq d_{\max}(\phi)$, with

$$d_{\min}(\phi) \triangleq \max \left(0, \frac{3 \cos \phi - \sqrt{9 \cos^2 \phi - 8}}{4} \right) \quad (33)$$

$$d_{\max}(\phi) \triangleq \max \left(0, \frac{3 \cos \phi + \sqrt{9 \cos^2 \phi - 8}}{4} \right) \quad (34)$$

otherwise, it monotonically decreases. For instance, if LTx, BTx, and LRx lie on the same line, i.e., $\phi = 0$, the function ΔC_3 monotonically decreases for $0 < d_{12}/d_{13} \leq 1/2$ and $d_{12}/d_{13} > 1$, while it increases when $1/2 < d_{12}/d_{13} < 1$. In this case, the capacity gain of the legacy system increases as the BTx gets closer and closer to either the LTx or the LRx.

If no significant channel variability occurs during the whole legacy transmission (i.e., the transmission duration of the codeword is comparable to the channel coherence time), a capacity in the ergodic sense does not exist. In this case, the concept of *capacity versus outage* has to be used [25], [26]. Assume that codewords extend over a single legacy frame and let the LTx encode data at a rate of R_s b/s/Hz, the outage probability of the legacy system is defined as

$$P_{\text{out},3} \triangleq P \left\{ \frac{1}{M} \sum_{m=0}^{M-1} \log \left[1 + \frac{\sigma_s^2}{\sigma_{v_3}^2} |\Psi_3(m)|^2 \right] < R_s \right\}. \quad (35)$$

However, for the problem at hand, $P_{\text{out},3}$ is hard to compute analytically and does not lead to easily interpretable results. Therefore, we resort to numerical simulations presented in Section VI to show the influence of the main system parameters on the outage probability of the legacy communication.

V. CAPACITY ANALYSIS OF THE BACKSCATTER SYSTEM

In the subsequent analysis, we separately consider two different network configurations. In the former case, we focus on the scenario where the intended recipient of the backscatter communication BRx and the legacy transmitter LTx are co-located, which is the situation considered in [4], [5]. In the latter case, we study the scenario where the BRx and the LTx are spatially-separated nodes, which is the situation considered in [3].

For simplicity, we remove the IBI in (17) by replacing condition (15) with the more restrictive one

$$L_b \geq \max(L_{14} + \theta_{14}, L_{24} + \theta_{24}, L_{12} + L_{24} + \theta_{12} + \theta_{24}) . \quad (36)$$

Under the assumption that

$$L_{12} + L_{24} + \theta_{12} + \theta_{24} \leq P - 1 \quad (37)$$

since only the first $L_{12} + L_{24} + \theta_{12} + \theta_{24}$ rows of $\tilde{\mathbf{C}}_{24}^{(0)} \tilde{\mathbf{C}}_{12}^{(1)}$ might not be zero, one thus has $\mathbf{R}_b \mathbf{\Sigma}_\nu \tilde{\mathbf{C}}_{24}^{(0)} \tilde{\mathbf{C}}_{12}^{(1)} = \mathbf{O}_{N \times P}$. Obviously, removing the IBI in (17) is not the best choice, since it does not allow one to exploit the entire channel energy. However, such a contribution becomes negligible for large values of N (i.e., P). Moreover, we assume herein that, in both the aforementioned cases, the number of samples L_b discarded from the received backscatter signal (14) is just equal to L_{cp} . We note that, when $L_{cp} = L_b$, then $N = M$ in (16)–(18). In this case, if (9) holds, the product $\tilde{\mathbf{C}}_{24}^{(0)} \tilde{\mathbf{C}}_{12}^{(0)}$ is a lower-triangular Toeplitz matrix having as first column $[\mathbf{0}_{\theta_{12} + \theta_{24}}^T, \mathbf{c}_{124}^T, \mathbf{0}_{P - L_{12} - L_{24} - \theta_{12} - \theta_{24} - 1}^T]^T$, where the vector $\mathbf{c}_{124} \in \mathbb{C}^{L_{12} + L_{24} + 1}$ collects the samples of the (linear) convolution between $\{c_{12}(\ell)\}_{\ell=0}^{L_{12}}$ and $\{c_{24}(\ell)\}_{\ell=0}^{L_{24}}$. This implies that the CP of the legacy system has to be designed to satisfy both inequalities (10) and (36). We would like to point out that, even though such an assumption is made only to keep the analysis relatively simple from a mathematical viewpoint, it is quite reasonable for small area networks.

A. The BRx and LTx are co-located

When the intended recipient of the backscatter signal and the legacy transmitter are co-located, the reference signal model can be obtained from (16)–(18) by replacing the subscript 4 with 1 and setting $\nu = 0$, which implies that $\mathbf{\Sigma}_\nu = \mathbf{I}_P$. In this case, the matrix $\tilde{\mathbf{C}}_{11}^{(0)}$ models a self-interference channel and $\tilde{\mathbf{C}}_{11}^{(0)} \mathbf{u}(n)$ represents direct leakage between the LTx transmit/receive chains and/or reflections by other objects in the environment [5].

It is worth observing that the symbol vector $\mathbf{s}(n)$ [and, thus, $\mathbf{u}(n)$] is perfectly known at the LTx, whereas the parameters $\{c_{121}, \theta_{12} + \theta_{21}\}$, which uniquely identify the matrix $\tilde{\mathbf{C}}_{21}^{(0)} \tilde{\mathbf{C}}_{12}^{(0)}$, and $\{c_{11}, \theta_{11}\}$, which uniquely identify the matrix $\tilde{\mathbf{C}}_{11}^{(0)}$, with $\mathbf{c}_{11} \triangleq [c_{11}(0), c_{11}(1), \dots, c_{11}(L_{11})]^T \in \mathbb{C}^{L_{11} + 1}$, can be estimated by allowing the insertion of training data within each packet of B symbols transmitted by

the BTx. More precisely, the self-interference parameters $\{\mathbf{c}_{11}, \theta_{11}\}$ can be estimated when there is no backscatter transmission: this can be obtained at the protocol level by employing a *silent period* of few symbols at the beginning of the packet [5], during which the BTx does not backscatter (i.e., $\alpha = 0$). Once \mathbf{c}_{11} and θ_{11} have been estimated by means of standard techniques [27], the self-interference contribution can be subtracted from (16). After the silent period, the BTx modulates training symbols on the backscatter signal [5], which can be used to estimate $\{\mathbf{c}_{121}, \theta_{12} + \theta_{21}\}$ through conventional methods [27].

After performing the DFT, one gets

$$\mathbf{r}_1(n) \triangleq \mathbf{W}_{\text{DFT}} \mathbf{R}_b \left[\tilde{\mathbf{r}}_1(n) - \tilde{\mathbf{C}}_{11}^{(0)} \mathbf{u}(n) \right] = \alpha \boldsymbol{\psi}(n) b(n) + \mathbf{v}_1(n) \quad (38)$$

where $\mathbf{W}_{\text{DFT}} \triangleq \mathbf{W}_{\text{IDFT}}^{-1} = \mathbf{W}_{\text{IDFT}}^{\text{H}}$ defines the unitary symmetric DFT matrix [12] and the nonzero entries of the diagonal matrix

$$\boldsymbol{\Psi}_{ik} \triangleq \text{diag}[\Psi_{ik}(0), \Psi_{ik}(1), \dots, \Psi_{ik}(M-1)] \quad (39)$$

are given by (13), $\boldsymbol{\psi}(n) \triangleq \boldsymbol{\psi}(n) \in \mathbb{C}^M$, and $\mathbf{v}_1(n) \triangleq \mathbf{W}_{\text{DFT}} \mathbf{R}_b \tilde{\mathbf{v}}_1(n) \in \mathbb{C}^M$. On the basis of the above discussion, the vector $\boldsymbol{\psi}(n)$ is assumed to be known at the LRx and, thus, *coherent* receiving rules can be adopted at the LRx. Moreover, we will omit the dependence on the frame index n hereinafter.

According to (38), given $\boldsymbol{\psi}$, a sufficient statistic for detecting b from \mathbf{r}_1 is given by the scalar

$$z_1 \triangleq \boldsymbol{\psi}^{\text{H}} \mathbf{r}_1 = \alpha \|\boldsymbol{\psi}\|^2 b + \boldsymbol{\psi}^{\text{H}} \mathbf{v}_1. \quad (40)$$

Since sufficient statistics preserve mutual information [23], [24], one has $I(b; \mathbf{r}_1, \boldsymbol{\psi}) = I(b; z_1, \boldsymbol{\psi})$. Therefore, the coherent ergodic capacity of (38) is given by

$$C_1 \triangleq \sup_{f(b) \in \mathcal{I}_b} \frac{I(b; z_1, \boldsymbol{\psi})}{M} \quad (\text{in b/s/Hz}) \quad (41)$$

where \mathcal{I}_b is the set of admissible input distributions $f(b)$ fulfilling *both* the variance constraint $E(|b|^2) = \sigma_b^2$ and, according to (5), the amplitude constraint $|b| \leq 1$ almost surely (a.s.). We remember that, since the average of a random variable cannot exceed its maximal value, the amplitude constraint implies that $\sigma_b^2 \leq 1$.

We observe that (40) is a conditionally Gaussian channel, given b and $\boldsymbol{\psi}$. It was shown in [28] that the capacity-achieving input distribution for conditional Gaussian channels under variance and amplitude constraints is *discrete* with a *finite* number of mass points. Therefore, there is no loss of generality in confining $f(b)$ to the set of discrete distributions. To this goal, let b be a discrete random variable taking on the value $\beta_q \in \mathcal{B}$ with probability p_q , for each $q \in \mathcal{Q}$, such that $|\beta_q| \leq 1$, $E(|b|^2) = \sigma_b^2$, and $\sum_{q \in \mathcal{Q}} p_q = 1$. Using the same arguments of Subsection IV, one gets

$$I(b; z_1, \boldsymbol{\psi}) = I(b; z_1 | \boldsymbol{\psi}) = \mathbb{E}_{\boldsymbol{\psi}} [I(b; z_1 | \boldsymbol{\psi} = \boldsymbol{\xi})]. \quad (42)$$

For the discrete input b , the mutual information $I(b; z_1 | \boldsymbol{\psi} = \boldsymbol{\xi})$ is given by

$$I(b; z_1 | \boldsymbol{\psi} = \boldsymbol{\xi}) = h(z_1 | \boldsymbol{\psi} = \boldsymbol{\xi}) - h(z_1 | b, \boldsymbol{\psi} = \boldsymbol{\xi}) \quad (43)$$

where

$$h(z_1 | \boldsymbol{\psi} = \boldsymbol{\xi}) = - \int_{\mathbb{C}} f_{z_1 | \boldsymbol{\psi} = \boldsymbol{\xi}}(x) \log f_{z_1 | \boldsymbol{\psi} = \boldsymbol{\xi}}(x) dx \quad (44)$$

is the differential entropy [23], [24] of $z_1 | \boldsymbol{\psi} = \boldsymbol{\xi}$, whereas

$$h(z_1 | b, \boldsymbol{\psi} = \boldsymbol{\xi}) = h(\alpha \|\boldsymbol{\psi}\|^2 b + \boldsymbol{\psi}^H \mathbf{v}_1 | b, \boldsymbol{\psi} = \boldsymbol{\xi}) = h(\boldsymbol{\psi}^H \mathbf{v}_1 | b, \boldsymbol{\psi} = \boldsymbol{\xi}) = h(\boldsymbol{\xi}^H \mathbf{v}_1) \quad (45)$$

turns out to be the differential entropy of $\boldsymbol{\xi}^H \mathbf{v}_1 \sim \mathcal{CN}(0, \sigma_{v_1}^2 \|\boldsymbol{\xi}\|^2)$, which is given (see, e.g., [29]) by $h(\boldsymbol{\xi}^H \mathbf{v}_1) = \log(\pi e \mathbb{E}[|\boldsymbol{\xi}^H \mathbf{v}_1|^2])$. It is noteworthy that, given $\boldsymbol{\psi} = \boldsymbol{\xi}$, the output distribution

$$f_{z_1 | \boldsymbol{\psi} = \boldsymbol{\xi}}(x) = \sum_{q=1}^Q p_q f_{z_1 | b = \beta_q, \boldsymbol{\psi} = \boldsymbol{\xi}}(x) \quad (46)$$

is a Gaussian mixture since $z_1 | b = \beta_q, \boldsymbol{\psi} = \boldsymbol{\xi} \sim \mathcal{CN}(\alpha \|\boldsymbol{\xi}\|^2 \beta_q, \sigma_{v_1}^2 \|\boldsymbol{\xi}\|^2)$. By virtue of (43), the optimization problem (41) is equivalent to the supremization of $\mathbb{E}_{\boldsymbol{\psi}}[h(z_1 | \boldsymbol{\psi} = \boldsymbol{\xi})]$ under the variance and amplitude constraints. However, the entropy $h(z_1 | \boldsymbol{\psi} = \boldsymbol{\xi})$ cannot be calculated in closed form due to the logarithm of a sum of exponential functions. As a consequence, an analytical expression for the optimizing probability mass function (pmf) of b is not available for the general case, neither there exists a closed-form formula for the corresponding capacity. Henceforth, upper and lower bounds on C_1 given by (41) are developed in the subsequent subsections.

1) *Upper bound on the capacity C_1* : An upper bound on the ergodic capacity C_1 can be obtained by resorting to the maximum-entropy theorem for complex random variables [29], which allows one to state that

$$h(z_1 | \boldsymbol{\psi} = \boldsymbol{\xi}) \leq \log(\pi e \mathbb{E}[|z_1|^2 | \boldsymbol{\psi} = \boldsymbol{\xi}]) = \log(\alpha^2 \sigma_b^2 \|\boldsymbol{\xi}\|^4 + \sigma_{v_1}^2 \|\boldsymbol{\xi}\|^2) . \quad (47)$$

By substituting (47) in (43) and accounting for (41)–(42), one gets the upper bound

$$C_1 \leq C_{1, \text{upper}} \triangleq \frac{1}{M} \mathbb{E}[\log(1 + \text{SNR}_{B,1} \Theta_{121})] \quad (48)$$

with $\text{SNR}_{B,1} \triangleq \alpha^2 \sigma_b^2 / \sigma_{v_1}^2$ and

$$\Theta_{121} \triangleq \sum_{m=0}^{M-1} |s^{(m)}|^2 |\Psi_{12}(m)|^2 |\Psi_{21}(m)|^2 . \quad (49)$$

It can be shown that, as Q grows, C_1 approaches $C_{1, \text{upper}}$ exponentially fast [30].

In the general case, the evaluation of the expectation in (48) is significantly complicated and will be numerically carried out in Section VI. Herein, we shall resort to a simpler asymptotic analysis by assuming that M is sufficiently large. It follows from the law of large numbers [31] that, as M gets large, the random

$$\begin{aligned}
-\log \int_{\mathbb{C}} \left[\sum_{q=1}^Q p_q \sqrt{f_{z_1 | b=\beta_q, \psi=\xi}(x)} \right]^2 dx &= -\log \sum_{q_1=1}^Q \sum_{q_2=1}^Q p_{q_1} p_{q_2} \int_{\mathbb{C}} \frac{1}{\pi \sigma_{v_1}^2 \|\xi\|^2} e^{-\frac{|x-\alpha\|\xi\|^2 \beta_{q_1}|^2 + |x-\alpha\|\xi\|^2 \beta_{q_2}|^2}{2\sigma_{v_1}^2 \|\xi\|^2}} dx \\
&= -\log \sum_{q_1=1}^Q \sum_{q_2=1}^Q p_{q_1} p_{q_2} e^{-\frac{\alpha^2 \|\xi\|^2 |\beta_{q_1} - \beta_{q_2}|^2}{4\sigma_{v_1}^2}} \int_{\mathbb{C}} \frac{1}{\pi \sigma_{v_1}^2 \|\xi\|^2} e^{-\frac{|x-\alpha\|\xi\|^2 \frac{\beta_{q_1} + \beta_{q_2}}{2}|^2}{\sigma_{v_1}^2 \|\xi\|^2}} dx \\
&= -\log \sum_{q_1=1}^Q \sum_{q_2=1}^Q p_{q_1} p_{q_2} e^{-\frac{\alpha^2 \|\xi\|^2 |\beta_{q_1} - \beta_{q_2}|^2}{4\sigma_{v_1}^2}} \quad (52)
\end{aligned}$$

variable Θ_{121}/M converges a.s. to $\sigma_s^2 \sigma_{12}^2 \sigma_{21}^2$. Hence, observing that, according to the considered path-loss model, it results that $\sigma_{12}^2 = \sigma_{21}^2$ since $d_{12} = d_{21}$, in the large M limit, one can write⁸

$$C_1 \leq C_{1,\text{upper}} |M \gg 1 \triangleq \frac{1}{M} \log \left(1 + \text{SNR}_{B,1} M \sigma_s^2 \sigma_{12}^4 \right) = \frac{1}{M} \log \left[1 + \text{SNR}_{B,1} \frac{M \sigma_s^2}{(d_{12}^2)^\eta} \right]. \quad (50)$$

Remark 7: When M is sufficiently large, the upper bound (48) is a monotonically increasing function of $\text{SNR}_{B,1}$ and $1/d_{12}$. In other words, significant high values of C_1 are obtained when the BTx reflects a large part of the incident EM wave and/or the BTx is very close to the LTx.

2) *Lower bound on the capacity C_1 :* By resorting to random coding arguments (see, e.g., [32]), it can be shown that the *cut-off rate*, which is defined as follows

$$R_1 \triangleq \max_{p_1, p_2, \dots, p_Q} -\log \int_{\mathbb{C}} \left[\sum_{q=1}^Q p_q \sqrt{f_{z_1 | b=\beta_q, \psi=\xi}(x)} \right]^2 dx \quad (51)$$

is a lower bound on $l(b; z_1 | \psi = \xi)$ at any SNR.

By using the properties of the logarithmic function, we observe that the objective function in (51) can be explicated as reported at the top of this page in (52), where the last but one equality is obtained by completion of the square in the exponent, whereas the last integral is 1 for any choice of the symbol set \mathcal{B} , since it is recognized as the integral of a univariate complex Gaussian pdf. Eq. (52) is valid for *any* finite-size symbol constellation, such as quadrature-amplitude modulation (QAM), PSK, orthogonal, lattice-type, or other. It is verified [32] that, for symbol constellations where the set of distances to other neighbors is invariant to the choice of the reference point, e.g., PSK and orthogonal modulations, the equiprobable assignment on the backscatter symbols (i.e., $p_q = 1/Q \forall q \in \mathcal{Q}$) maximizes (52). Therefore, remembering

⁸For any value of M , eq. (50) is as an upper bound on (48): by Jensen's inequality, $\mathbb{E}[\log(1 + \text{SNR}_{B,1} \Theta_{121})] \leq \log[1 + \text{SNR}_{B,1} \mathbb{E}(\Theta_{121})]$, with $\mathbb{E}(\Theta_{121}) = M \sigma_s^2 \sigma_{12}^2 \sigma_{21}^2$.

(41), (42), and (51), one yields $C_1 \geq C_{1,\text{lower}}$, with

$$C_{1,\text{lower}} \triangleq \frac{\log Q - \mathbb{E} \left[\log \left(1 + \sum_{q=2}^Q e^{-\Theta_{121} \text{SNR}_{B,1} \frac{|\beta_1 - \beta_q|^2}{4\sigma_b^2}} \right) \right]}{M} \quad (53)$$

where $\text{SNR}_{B,1}$ and Θ_{121} have been defined in Subsection V-A1. The further lower bound

$$C_{1,\text{lower}} \geq \frac{\log Q - \mathbb{E} \left[\log \left(1 + (Q-1) e^{-\Theta_{121} \text{SNR}_{B,1} \frac{\delta_{\min}^2}{4\sigma_b^2}} \right) \right]}{M} \quad (54)$$

can be obtained by noting that $|\beta_1 - \beta_q|^2 \geq \delta_{\min}^2$ for each $q \in \mathcal{Q}$, where $\delta_{\min} \triangleq \min_{q_1 \neq q_2 \in \mathcal{Q}} |\beta_{q_1} - \beta_{q_2}|$ is the minimum distance between any two data symbols in the signal constellation \mathcal{B} . By invoking again the law of large numbers [31], in the large M limit, the following asymptotic expressions of $C_{1,\text{lower}}$ and its lower bound (54) hold

$$C_{1,\text{lower}|M \gg 1} \triangleq \frac{\log Q - \log \left(1 + \sum_{q=2}^Q e^{-\frac{\sigma_s^2 M \text{SNR}_{B,1} |\beta_1 - \beta_q|^2}{4\sigma_b^2 (d_{12}^2)^\eta}} \right)}{M} \geq \frac{\log Q - \log \left(1 + (Q-1) e^{-\frac{\sigma_s^2 M \text{SNR}_{B,1} \delta_{\min}^2}{4\sigma_b^2 (d_{12}^2)^\eta}} \right)}{M}. \quad (55)$$

Remark 8: The lower bound $C_{1,\text{lower}}$ approaches $(\log Q)/M$ as $\text{SNR}_{B,1}$ increases or the distance d_{12} between the LTx and the BTx decreases. On the other hand, when $x \rightarrow 0$, the function $\log(1 + A e^{-Bx})$ can be approximated using the first two terms of its Mac Laurin series expansion, i.e., $\log(1 + A e^{-Bx}) \approx \log(1 + A) - AB(1 + A)^{-1}x$, in the low-SNR regime $\text{SNR}_{B,1} \rightarrow 0$ or when $d_{12} \rightarrow +\infty$, hence getting

$$C_{1,\text{lower}|M \gg 1} \rightarrow \left(1 - \frac{1}{Q} \right) \frac{\sigma_s^2 \text{SNR}_{B,1} \delta_{\min}^2}{4\sigma_b^2 (d_{12}^2)^\eta} \quad (56)$$

that is, the capacity increases linearly with $\text{SNR}_{B,1}$ and monotonically decreases as the distance d_{12} raises.

B. The BRx and LTx are spatially-separated nodes

We consider the scenario where the LTx and BRx are spatially-separated nodes, which is the situation considered in [3]. In this case, taking into account the aforementioned simplifying assumptions (36) and $L_{\text{cp}} = L_b$, the reference signal model (16)–(18) becomes

$$\mathbf{R}_b \tilde{\mathbf{r}}_4(n) = \alpha \left[e^{j\frac{2\pi}{M}\nu n P} \mathbf{R}_b \boldsymbol{\Sigma}_\nu \tilde{\mathbf{C}}_{24}^{(0)} \tilde{\mathbf{C}}_{12}^{(0)} \mathbf{u}(n) \right] b(n) + \mathbf{d}_4(n) \quad (57)$$

with

$$\mathbf{d}_4(n) = e^{j\frac{2\pi}{M}\nu n P} \mathbf{R}_b \boldsymbol{\Sigma}_\nu \tilde{\mathbf{C}}_{14}^{(0)} \mathbf{u}(n) + \mathbf{R}_b \tilde{\mathbf{v}}_4(n) \in \mathbb{C}^M. \quad (58)$$

Compared to the case studied in Subsection V-A, there are two key differences: (i) the receiver has no knowledge of the data block $\mathbf{u}(n) = \mathbf{T}_{\text{cp}} \mathbf{W}_{\text{IDFT}} \mathbf{s}(n)$ transmitted by the LTx; (ii) there is a nonzero CFO ν between the received carrier and the local sinusoids used for signal demodulation.

If the BRx does not have any *a priori* knowledge regarding the legacy transmission, recovery of $b(n)$ can be accomplished at the BRx by resorting to *noncoherent* detection rules. The noncoherent ergodic capacity of (57)–(58) is given by the supremum of the mutual information $I[b; \mathbf{R}_b \tilde{\mathbf{r}}_4(n)]$ over the set \mathcal{I}_b of admissible input distribution satisfying both the variance and amplitude constraints. Evaluation of the noncoherent ergodic capacity with only a variance constraint has been studied in [33], [34], [35] under the assumption that the channel matrix [corresponding to $e^{j\frac{2\pi}{M}\nu nP} \mathbf{R}_b \Sigma_\nu \tilde{\mathbf{C}}_{24}^{(0)} \tilde{\mathbf{C}}_{12}^{(0)} \mathbf{u}(n)$ in our framework] and noise [corresponding to $\mathbf{d}_4(n)$ in our framework] follow a Gaussian distribution. In the case under study, evaluation of the noncoherent ergodic capacity is further complicated by the non-Gaussian nature of both $e^{j\frac{2\pi}{M}\nu nP} \mathbf{R}_b \Sigma_\nu \tilde{\mathbf{C}}_{24}^{(0)} \tilde{\mathbf{C}}_{12}^{(0)} \mathbf{u}(n)$ and $\mathbf{d}_4(n)$, as well as by the amplitude constraint $|b| \leq 1$.

To avoid incurring the data-rate penalty of the noncoherent communication scheme, we study the case where, besides having knowledge of the training symbols transmitted by the BTx, the BRx additionally knows the pilot symbols sent by the LTx in each frame. Under this assumption, following the same protocol outlined in Subsubsection V-A, during the silent period of the BTx (i.e., when $\alpha = 0$), the BRx receives the signal $\mathbf{d}_4(n)$, from which it can estimate the CFO ν and the parameters of the channel matrix $\tilde{\mathbf{C}}_{14}^{(0)}$ by resorting to standard estimators [20], [27]. However, it should be observed that the interference contribution $e^{j\frac{2\pi}{M}\nu nP} \mathbf{R}_b \Sigma_\nu \tilde{\mathbf{C}}_{14}^{(0)} \mathbf{u}(n)$ cannot be subtracted from (57) since the information-bearing data in $\mathbf{u}(n)$ are unknown at the BRx (only the pilots and their locations are assumed to be known). Once ν has been estimated, the vector $\tilde{\mathbf{r}}_4(n)$ can be counter-rotated at the angular speed $2\pi\nu/M$, thus yielding

$$\mathbf{r}_4 \triangleq \mathbf{R}_b \tilde{\mathbf{r}}_4 = \alpha (\mathbf{W}_{\text{IDFT}} \Psi_{12} \Psi_{24} \mathbf{s}) b + \mathbf{W}_{\text{IDFT}} \Psi_{14} \mathbf{s} + \mathbf{v}_4 \quad (59)$$

with $\mathbf{v}_4 \triangleq \mathbf{R}_b \tilde{\mathbf{v}}_4 \in \mathbb{C}^M$, where $\mathbf{s} \sim \mathcal{CN}(\mathbf{0}_M, \sigma_s^2 \mathbf{I}_M)$ is the capacity-achieving distribution for the legacy system (see Section IV) and we have again omitted the dependence of the frame index n . Since $\mathbf{\Omega}_{124} \triangleq \Psi_{12} \Psi_{24} \in \mathbb{C}^{M \times M}$ and $\mathbf{\Omega}_{14} \triangleq \Psi_{14} \in \mathbb{C}^{M \times M}$ are known but \mathbf{s} is unknown, we refer to (59) as the *partially-coherent* channel model. The partially-coherent ergodic capacity of (59) is given by

$$C_4 \triangleq \sup_{f(b) \in \mathcal{I}_b} I(b; \mathbf{r}_4, \mathbf{\Omega}_{124}, \mathbf{\Omega}_{14}) \quad (60)$$

where \mathcal{I}_b is the set of admissible input distributions fulfilling $E(|b|^2) = \sigma_b^2$ and $|b| \leq 1$ a.s., and

$$I(b; \mathbf{r}_4, \mathbf{\Omega}_{124}, \mathbf{\Omega}_{14}) = I(b; \mathbf{r}_4 | \mathbf{\Omega}_{124}, \mathbf{\Omega}_{14}) = \mathbb{E}_{\mathbf{\Omega}_{124}, \mathbf{\Omega}_{14}} [I(b; \mathbf{r}_4 | \mathbf{\Omega}_{124} = \mathbf{\Xi}_{124}, \mathbf{\Omega}_{14} = \mathbf{\Xi}_{14})] . \quad (61)$$

Similarly to the case studied in Subsection V-A, closed-form expressions for C_4 and the corresponding capacity-achieving discrete distribution $f(b)$ are unavailable. Therefore, we derive upper and lower bounds on C_4 .

1) *Upper bound on the capacity C_4* : An upper bound on C_4 can be obtained by assuming that the BRx has the additional perfect knowledge of \mathbf{s} . Indeed, by using the chain rule for mutual information [23], [24], it can be proven that

$$I(b; \mathbf{r}_4 | \mathbf{\Omega}_{124}, \mathbf{\Omega}_{14}, \mathbf{s}) = I(b; \mathbf{r}_4, | \mathbf{\Omega}_{124}, \mathbf{\Omega}_{14}) + I(b; \mathbf{s} | \mathbf{r}_4, \mathbf{\Omega}_{124}, \mathbf{\Omega}_{14}) \geq I(b; \mathbf{r}_4, | \mathbf{\Omega}_{124}, \mathbf{\Omega}_{14}) \quad (62)$$

since $I(b; \mathbf{r}_4, | \mathbf{\Omega}_{124}, \mathbf{\Omega}_{14}) \geq 0$ by definition. Moreover, because subtracting a constant does not change mutual information [23], [24], one has

$$\begin{aligned} I(b; \mathbf{r}_4 | \mathbf{\Omega}_{124}, \mathbf{\Omega}_{14}, \mathbf{s}) &= I(b; \mathbf{r}_4 - \mathbf{W}_{\text{IDFT}} \mathbf{\Omega}_{14} \mathbf{s} | \mathbf{\Omega}_{124}, \mathbf{\Omega}_{14}, \mathbf{s}) \\ &= \mathbb{E}_{\mathbf{\Omega}_{124}, \mathbf{\Omega}_{14}, \mathbf{s}} [I(b; \mathbf{r}_4 - \mathbf{W}_{\text{IDFT}} \mathbf{\Omega}_{14} \mathbf{s} | \mathbf{\Omega}_{124} = \mathbf{\Xi}_{124}, \mathbf{\Omega}_{14} = \mathbf{\Xi}_{14}, \mathbf{s} = \mathbf{a})] \end{aligned} \quad (63)$$

that is, since the BRx knows $\mathbf{\Omega}_{14}$ and \mathbf{s} , it can estimate b by subtracting $\mathbf{W}_{\text{IDFT}} \mathbf{\Omega}_{14} \mathbf{s}$ from (59), hence yielding $\hat{\mathbf{r}}_4 \triangleq \mathbf{r}_4 - \mathbf{W}_{\text{IDFT}} \mathbf{\Omega}_{14} \mathbf{s} = \alpha \mathbf{W}_{\text{IDFT}} \mathbf{\Omega}_{124} \mathbf{s} b + \mathbf{v}_4$. It follows that

$$\begin{aligned} I(b; \mathbf{r}_4 - \mathbf{\Omega}_{14} \mathbf{s} | \mathbf{\Omega}_{124} = \mathbf{\Xi}_{124}, \mathbf{\Omega}_{14} = \mathbf{\Xi}_{14}, \mathbf{s} = \mathbf{a}) &= h(\hat{\mathbf{r}}_4 | \mathbf{\Omega}_{124} = \mathbf{\Xi}_{124}, \mathbf{\Omega}_{14} = \mathbf{\Xi}_{14}, \mathbf{s} = \mathbf{a}) \\ &\quad - h(\hat{\mathbf{r}}_4 | b, \mathbf{\Omega}_{124} = \mathbf{\Xi}_{124}, \mathbf{\Omega}_{14} = \mathbf{\Xi}_{14}, \mathbf{s} = \mathbf{a}) \end{aligned} \quad (64)$$

where $h(\hat{\mathbf{r}}_4 | b, \mathbf{\Omega}_{124} = \mathbf{\Xi}_{124}, \mathbf{\Omega}_{14} = \mathbf{\Xi}_{14}, \mathbf{s} = \mathbf{a}) = h(\mathbf{v}_4) = M \log(\pi e \sigma_{v_4}^2)$. As a consequence of the maximum-entropy theorem for complex random variables [29], one can obtain a further upper bound on (64) by observing that

$$\begin{aligned} h(\hat{\mathbf{r}}_4 | \mathbf{\Omega}_{124} = \mathbf{\Xi}_{124}, \mathbf{\Omega}_{14} = \mathbf{\Xi}_{14}, \mathbf{s} = \mathbf{a}) &\leq \log \{ (\pi e)^M \det(\mathbb{E} [\hat{\mathbf{r}}_4 \hat{\mathbf{r}}_4^H | \mathbf{\Omega}_{124} = \mathbf{\Xi}_{124}, \mathbf{\Omega}_{14} = \mathbf{\Xi}_{14}, \mathbf{s} = \mathbf{a}]) \} \\ &= \log [(\pi e \sigma_{v_4}^2)^M (1 + \text{SNR}_{\text{B},4} \|\mathbf{\Xi}_{124} \mathbf{a}\|^2)] \end{aligned} \quad (65)$$

with $\text{SNR}_{\text{B},4} \triangleq \alpha^2 \sigma_b^2 / \sigma_{v_4}^2$, where we have used the facts [11] that: (i) $\det(\mathbf{A} \mathbf{B}) = \det(\mathbf{A}) \det(\mathbf{B})$ for arbitrary nonsingular matrices $\mathbf{A} \in \mathbb{C}^{n \times n}$ and $\mathbf{B} \in \mathbb{C}^{n \times n}$; (ii) $\det(\mathbf{W}_{\text{IDFT}}) \det(\mathbf{W}_{\text{DFT}}) = 1$; (iii) for arbitrary vectors $\mathbf{x} \in \mathbb{C}^n$ and $\mathbf{y} \in \mathbb{C}^n$, $\det(\mathbf{I}_n + \mathbf{x} \mathbf{y}^H) = 1 + \mathbf{x}^H \mathbf{y}$. Henceforth, accounting for (62)–(65), it results from (60) that

$$C_4 \leq C_{4,\text{upper}} \triangleq \frac{1}{M} \mathbb{E} [\log (1 + \text{SNR}_{\text{B},4} \Theta_{124})] \quad (66)$$

with

$$\Theta_{124} \triangleq \sum_{m=0}^{M-1} |s^{(m)}|^2 |\Psi_{12}(m)|^2 |\Psi_{24}(m)|^2. \quad (67)$$

Such an upper bound is achieved when the BRx is able to reliably estimate the legacy symbols and $Q \rightarrow +\infty$. It should be noted that (66) is similar to (48). Thus, the asymptotic analysis reported in Subsection V-A1 soon after (48) can be applied to (66) with minor modifications. In particular, in the large M limit, one obtains

$$C_4 \leq C_{4,\text{upper}}|_{M \gg 1} \triangleq \frac{1}{M} \log (1 + \text{SNR}_{\text{B},4} M \sigma_s^2 \sigma_{12}^2 \sigma_{24}^2) = \frac{1}{M} \log \left[1 + \text{SNR}_{\text{B},4} \frac{M \sigma_s^2}{(d_{12} d_{24})^\eta} \right] \quad (68)$$

$$\begin{aligned}
R_4 &= -\log \sum_{q_1=1}^Q \sum_{q_2=1}^Q \frac{1}{Q^2} \int_{\mathbb{C}^M} \frac{e^{-\frac{\mathbf{x}^H [\mathbf{K}_4^{-1}(\beta_{q_1}) + \mathbf{K}_4^{-1}(\beta_{q_2})] \mathbf{x}}{2}}}{\pi^M \sqrt{\det [\mathbf{K}_4(\beta_{q_1})] \det [\mathbf{K}_4(\beta_{q_2})]}} d\mathbf{x} \\
&= -\log \sum_{q_1=1}^Q \sum_{q_2=1}^Q \frac{\det \left\{ 2 [\mathbf{K}_4^{-1}(\beta_{q_1}) + \mathbf{K}_4^{-1}(\beta_{q_2})]^{-1} \right\}}{Q^2 \sqrt{\det [\mathbf{K}_4(\beta_{q_1})] \det [\mathbf{K}_4(\beta_{q_2})]}} \int_{\mathbb{C}^M} \frac{e^{-\frac{\mathbf{x}^H [\mathbf{K}_4^{-1}(\beta_{q_1}) + \mathbf{K}_4^{-1}(\beta_{q_2})] \mathbf{x}}{2}}}{\pi^M \det \left\{ 2 [\mathbf{K}_4^{-1}(\beta_{q_1}) + \mathbf{K}_4^{-1}(\beta_{q_2})]^{-1} \right\}} d\mathbf{x} \\
&= \log Q - \log \left[1 + \frac{2^M}{Q} \sum_{q_1=1}^Q \sum_{\substack{q_2=1 \\ q_2 \neq q_1}}^Q \frac{1}{\sqrt{\det [\mathbf{R}_4(\beta_{q_1})] \det [\mathbf{R}_4(\beta_{q_2})] \det [\mathbf{R}_4^{-1}(\beta_{q_1}) + \mathbf{R}_4^{-1}(\beta_{q_2})]}} \right]
\end{aligned} \tag{71}$$

where, by virtue of the Carnot's cosine law, the distances d_{12} and d_{24} are related by $d_{24} = (d_{12}^2 + d_{14}^2 - 2 d_{12} d_{14} \cos \theta)^{1/2}$, with θ being the angle opposite to the $2 \rightarrow 4$ link (see Fig. 1).

Remark 9: For a fixed value of d_{14} and θ , the capacity $C_{4,\text{upper}}|_{M \gg 1}$ as a function of d_{12} exhibits the same behavior of ΔC_3 (see Remark 6). In a nutshell, when $\theta \in \mathcal{A}$, the upper bound $C_{4,\text{upper}}|_{M \gg 1}$ is a strictly decreasing function of d_{12}/d_{14} , whereas, when $\theta \notin \mathcal{A}$, it monotonically increases for $d_{\min}(\theta) \leq d_{12}/d_{14} \leq d_{\max}(\theta)$, otherwise, it monotonically decreases. In other words, if the BRx reliably estimates the legacy symbols, in the former case, the capacity C_4 of the backscatter system decreases while the BTx is departing from the LTx, whereas, in latter one, it increases as the BTx approaches to either the LTx or an intermediate point between the LTx and the BRx.

2) *Lower bound on the capacity C_4 :* As in Subsection V-A2, we rely on the fact that

$$R_4 \leq I(b; \mathbf{r}_4 | \boldsymbol{\Omega}_{124} = \boldsymbol{\Xi}_{124}, \boldsymbol{\Omega}_{14} = \boldsymbol{\Xi}_{14}) \tag{69}$$

where R_4 is the cut-off rate when the backscatter symbols are assumed to be equiprobable, that is,

$$R_4 \triangleq -\log \int_{\mathbb{C}^M} \left[\frac{1}{Q} \sum_{q=1}^Q \sqrt{f_{\mathbf{r}_4 | b=\beta_q, \boldsymbol{\Omega}_{124}=\boldsymbol{\Xi}_{124}, \boldsymbol{\Omega}_{14}=\boldsymbol{\Xi}_{14}}(\mathbf{x})} \right]^2 d\mathbf{x}. \tag{70}$$

Eq. (59) shows that $\mathbf{r}_4 | b = \beta_q, \boldsymbol{\Omega}_{124} = \boldsymbol{\Xi}_{124}, \boldsymbol{\Omega}_{14} = \boldsymbol{\Xi}_{14} \sim \mathcal{CN}[\mathbf{0}_M, \mathbf{K}_4(\beta_q, \boldsymbol{\Xi}_{124}, \boldsymbol{\Xi}_{14})]$, with $\mathbf{K}_4(\beta_q, \boldsymbol{\Xi}_{124}, \boldsymbol{\Xi}_{14}) \triangleq \mathbb{E}(\mathbf{r}_4 \mathbf{r}_4^H | b = \beta_q, \boldsymbol{\Omega}_{124} = \boldsymbol{\Xi}_{124}, \boldsymbol{\Omega}_{14} = \boldsymbol{\Xi}_{14}) = \mathbf{W}_{\text{IDFT}} \mathbf{R}_4(\beta_q, \boldsymbol{\Xi}_{124}, \boldsymbol{\Xi}_{14}) \mathbf{W}_{\text{DFT}}$, where $\mathbf{R}_4(\beta_q, \boldsymbol{\Xi}_{124}, \boldsymbol{\Xi}_{14}) \triangleq \alpha^2 \sigma_s^2 \boldsymbol{\Xi}_{124} \boldsymbol{\Xi}_{124}^* |\beta_q|^2 + \alpha \sigma_s^2 \boldsymbol{\Xi}_{124} \boldsymbol{\Xi}_{14}^* \beta_q + \alpha \sigma_s^2 \boldsymbol{\Xi}_{124}^* \boldsymbol{\Xi}_{14} \beta_q^* + \sigma_s^2 \boldsymbol{\Xi}_{14} \boldsymbol{\Xi}_{14}^* + \sigma_{v_4}^2 \mathbf{I}_M$ is a diagonal matrix. By using the properties of the determinant [11], we observe that R_4 can be explicated as reported at the top of this page in (71), where we have omitted to explicitly indicate the

$$C_4 \geq C_{4,\text{lower}} \triangleq \frac{\log Q - \mathbb{E} \left[\log \left(1 + \frac{2^M}{Q} \sum_{q_1=1}^Q \sum_{\substack{q_2=1 \\ q_2 \neq q_1}}^Q \prod_{m=0}^{M-1} \frac{\sqrt{\Lambda_{q_1}(m) \Lambda_{q_2}(m)}}{\Lambda_{q_1}(m) + \Lambda_{q_2}(m)} \right) \right]}{M} \quad (72)$$

dependence of $\mathbf{K}_4(\cdot)$ and $\mathbf{R}_4(\cdot)$ on Ξ_{124} and Ξ_{14} , and the last integral is the hypervolume of a multivariate complex Gaussian pdf. By virtue of (61) and (69), the capacity (60) is lower bounded as shown at the top of this page in (72), with

$$\Lambda_q(m) \triangleq \alpha^2 \sigma_s^2 |\Psi_{12}(m)|^2 |\Psi_{24}(m)|^2 |\beta_q|^2 + 2\alpha \sigma_s^2 \Re \{ \Psi_{12}(m) \Psi_{24}(m) \Psi_{14}^*(m) \beta_q \} + \sigma_s^2 |\Psi_{14}(m)|^2 + \sigma_{v_4}^2. \quad (73)$$

In addition to noise, another additive source of performance degradation is the interference generated by the legacy system over the $1 \rightarrow 4$ link, which may seriously limit the achievable rates of the backscatter system in the high-SNR region.

Remark 10: It is verified from (72) that $C_{4,\text{lower}} \rightarrow 0$ if $\Lambda_{q_1}(m) \rightarrow \Lambda_{q_2}(m)$ for each $q_1 \neq q_2 \in \mathcal{Q}$. For instance, this happens when the second and third summands in the RHS of (73) are dominant over the first and second ones, i.e., when interference and/or noise dominates the backscatter signal.

The dependence of the $C_{4,\text{lower}}$ on the distance d_{12} between the LTx and the BTx is not easily deduced from (72) and such a behavior will be studied numerically in Section VI. To gain some useful insights, we consider the special case of a 2-PSK (i.e., BPSK), where $\beta_1 = -\beta_2 = 1$. In this case, eq. (72) becomes

$$\begin{aligned} C_{4,\text{lower}}^{\text{bpsk}} &= \frac{1}{M} - \frac{1}{M} \mathbb{E} \left\{ \log \left[1 + \prod_{m=0}^{M-1} \sqrt{1 - \frac{\Lambda_1^2(m)}{\Lambda_2^2(m)}} \right] \right\} \geq \frac{1}{M} - \frac{1}{M} \log \left\{ 1 + \sqrt{\mathbb{E} \left[\prod_{m=0}^{M-1} \left(1 - \frac{\Lambda_1^2(m)}{\Lambda_2^2(m)} \right) \right]} \right\} \\ &\approx \frac{1}{M} - \frac{1}{M} \log \left\{ 1 + \sqrt{\prod_{m=0}^{M-1} \left(1 - \mathbb{E} \left[\frac{\Lambda_1^2(m)}{\Lambda_2^2(m)} \right] \right)} \right\} \end{aligned} \quad (74)$$

with

$$\Lambda_1(m) \triangleq \alpha^2 \sigma_s^2 |\Psi_{12}(m)|^2 |\Psi_{24}(m)|^2 + \sigma_s^2 |\Psi_{14}(m)|^2 + \sigma_{v_4}^2 \quad (75)$$

$$\Lambda_2(m) \triangleq 2\alpha \sigma_s^2 \Re \{ \Psi_{12}(m) \Psi_{24}(m) \Psi_{14}^*(m) \} \quad (76)$$

where the inequality in (74) comes from the application of the Jensen's inequality to the concave function $\log(1 + \sqrt{x})$, whereas the approximation is obtained by neglecting the correlation between the random variables $\Lambda_1^2(m_1)/\Lambda_2^2(m_1)$ and $\Lambda_1^2(m_2)/\Lambda_2^2(m_2)$, for $m_1 \neq m_2 \in \mathcal{M}$. The first-order Taylor expansion of

$\mathbb{E} [\Lambda_1^2(m)/\Lambda_2^2(m)]$ leads to the further approximation⁹ $\mathbb{E} [\Lambda_1^2(m)/\Lambda_2^2(m)] \approx \mathbb{E}[\Lambda_1^2(m)]/\mathbb{E}[\Lambda_2^2(m)]$, where in the low-noise regime $\sigma_{v_4}^2/\sigma_s^2 \rightarrow 0$, one has

$$J(d_{12}) \triangleq \lim_{\sigma_{v_4}^2/\sigma_s^2 \rightarrow 0} \frac{\mathbb{E}[\Lambda_1^2(m)]}{\mathbb{E}[\Lambda_2^2(m)]} = \frac{1}{1 + \frac{2}{D(d_{12})} + D(d_{12})} \quad (77)$$

where $D(d_{12}) \triangleq (d_{12} d_{24}/d_{14})^\eta / \alpha^2$ is independent of m , with $d_{24} = (d_{12}^2 + d_{14}^2 - 2 d_{12} d_{14} \cos \theta)^{1/2}$. Therefore, when $\sigma_{v_4}^2/\sigma_s^2 \rightarrow 0$, it results from (74) that¹⁰

$$C_{4,\text{lower}}^{\text{bpsk}} \gtrsim \frac{1}{M} - \frac{1}{M} \log \left\{ 1 + [1 - J(d_{12})]^{M/2} \right\}. \quad (78)$$

Remark 11: For a fixed value of d_{14} and θ (see Fig. 1), by using standard concepts of mathematical analysis,¹¹ it can be shown that, if $\theta \in \mathcal{A}$, then $J(d_{12})$ is a *unimodal* function, exhibiting a maximum when $D(d_{12}) = \sqrt{2}$. On the other hand, when $\theta \notin \mathcal{A}$, the function $J(d_{12})$ is *multimodal* having multiple local extrema points.

VI. NUMERICAL PERFORMANCE ANALYSIS

We present the Monte Carlo numerical analysis of the considered ambient backscatter network to validate and complete our theoretical analysis, with reference to both legacy and backscatter systems. All the ensemble averages (with respect to all the relevant fading channels and information-bearing symbols) and the outage probability of the legacy system are evaluated through 10^6 independent Monte Carlo runs.

In all the experiments, we adopted the following simulation setting. With reference to the Cartesian plane in Fig. 1, all the distances are normalized with respect to $d_{13} = 1$. Specifically, the nodes 1 (LTx) and 3 (LRx) have coordinates equal to $(-0.5, 0)$ and $(0.5, 0)$, respectively. In all the plots where the distance d_{12} varies, the node 2 (BTx) moves along the line joining the nodes 1 and 2 (see Fig. 1). The multicarrier legacy system employs $M = 32$ subcarriers and a CP of length $L_{\text{cp}} = 8$. The legacy symbols are generated according to the corresponding capacity-achieving distribution $\mathbf{s} \sim \mathcal{CN}(\mathbf{0}_M, \sigma_s^2 \mathbf{I}_M)$, with $\sigma_s^2 = 1$. On the other hand, the symbols transmitted by the backscatter device are equiprobably drawn from BPSK, 4-PSK (i.e., QPSK), and quaternary amplitude-shift keying (ASK) signal constellations, with average energy $\sigma_b^2 = 1$. The order of the discrete-time channels between the nodes is set equal to $L_{13} = L_{12} = L_{23} = 3$, whereas the corresponding time offsets are fixed to $\theta_{13} = \theta_{12} = \theta_{23} = 1$, respectively. Moreover, the

⁹Let $f(X, Y) \triangleq X/Y$ be a transformation of the two random variables X and Y . Let $\mu_X \triangleq \mathbb{E}(X)$ and $\mu_Y \triangleq \mathbb{E}(Y)$, the first-order Taylor approximation for $\mathbb{E}[f(X, Y)]$ is given by $\mathbb{E}[f(X, Y)] = f(\mu_X, \mu_Y) + \mathbb{E}[f'_x(\mu_X, \mu_Y)(X - \mu_X)] + \mathbb{E}[f'_y(\mu_X, \mu_Y)(Y - \mu_Y)] = f(\mu_X, \mu_Y) = \mu_X/\mu_Y$, where $f'_x(\cdot)$ and $f'_y(\cdot)$ are the partial derivatives of the function $f(x, y)$ with respect to the real-valued variables x and y , respectively.

¹⁰Using similar bounding/approximation techniques, a lower bound on $C_{4,\text{lower}}$ can be obtained for an arbitrary M -ary backscatter signal constellation, which however does not lend itself to easily interpretable results.

¹¹Details are omitted in the interest of saving space.

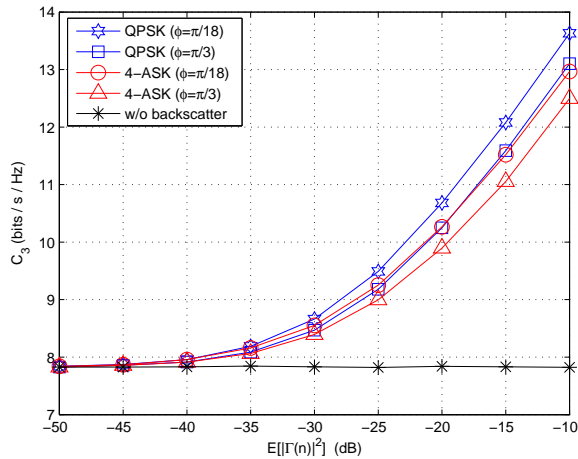


Figure 3. Ergodic capacity of the legacy system versus $\mathbb{E}[|\Gamma(n)|^2] = \alpha^2$ for two backscatter signal constellations and two values of the angle ϕ .

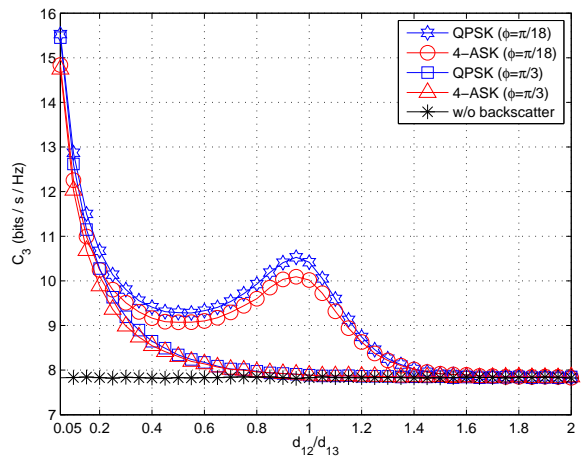


Figure 4. Ergodic capacity of the legacy system versus d_{12}/d_{13} for two backscatter signal constellations and two values of the angle ϕ .

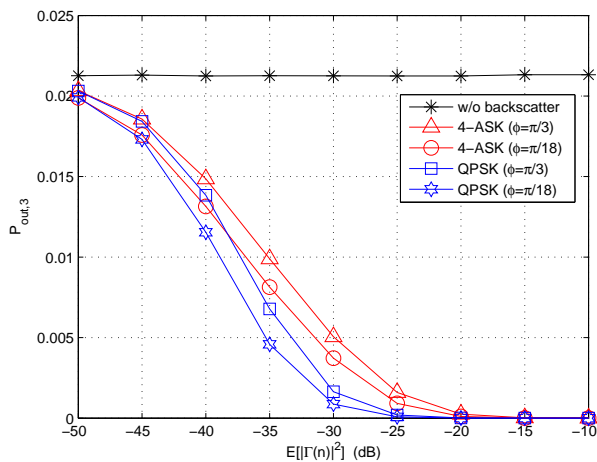


Figure 5. Outage probability of the legacy system versus $\mathbb{E}[|\Gamma(n)|^2] = \alpha^2$ for two backscatter signal constellations and two values of the angle ϕ .

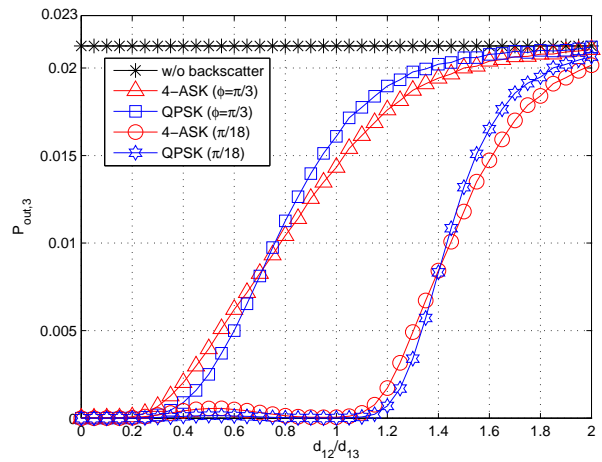


Figure 6. Outage probability of the legacy system versus d_{12}/d_{13} for two backscatter signal constellations and two values of the angle ϕ .

path-loss exponent is chosen equal to $\eta = 3$. For the evaluation of the outage probability of the legacy system, we chose $R_s = 6$ b/s/Hz in (35).

A. Performance of the legacy system

Figs. 3 and 4 depict the ergodic capacity C_3 of the legacy system given by (22), in comparison with the ergodic capacity (24) when the backscatter system is in sleep mode (referred to as “w/o backscatter”), with $\text{SNR}_L = \sigma_s^2/\sigma_{v_3}^2 = 20$ dB and $\phi \in \{\pi/18, \pi/3\}$. In Fig. 3, the capacity values are reported as a function of the *mean square power wave reflection coefficient* $\mathbb{E}[|\Gamma(n)|^2] = \alpha^2 \sigma_b^2$, with $d_{12}/d_{13} = 0.2$, whereas they are plotted against d_{12}/d_{13} in Fig. 4, with $\mathbb{E}[|\Gamma(n)|^2] = -20$ dB.

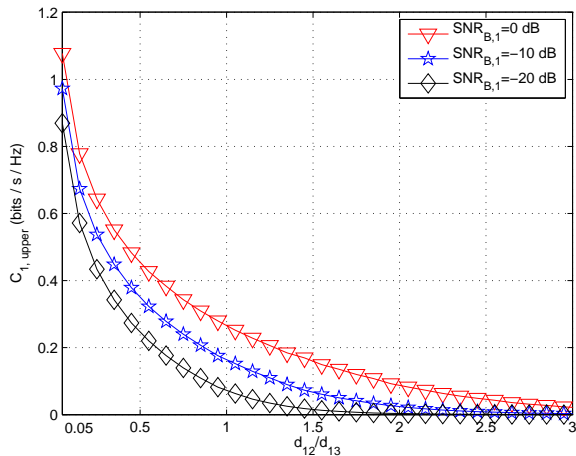


Figure 7. Best-case ergodic capacity of the backscatter system versus d_{12}/d_{13} for different values of $\text{SNR}_{B,1}$ (LTx and BRx are co-located).

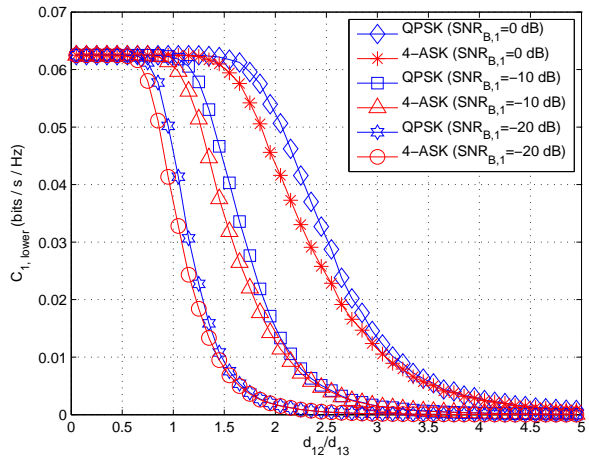


Figure 8. Worst-case ergodic capacity of the backscatter system versus d_{12}/d_{13} for different values of $\text{SNR}_{B,1}$ (LTx and BRx are co-located).

As announced in Remark 4, the capacity of the legacy system cannot degrade in the presence of the backscatter transmission, in each operative condition. In particular, the performance gain $\Delta C_3 = C_3 - C_3|_{\alpha=0}$ becomes relevant either when $\mathbb{E}[|\Gamma(n)|^2]$ is sufficiently large (see Remark 5) or the BTx is very close to the LTx. In particular, it is seen that, for a fixed Q , the choice of the backscatter signal constellation (ASK or PSK) does not lead to significantly different values of C_3 . Moreover, results of Fig. 4 confirm the trends analytically predicted in Remark 6, by showing that C_3 monotonically decreases as the BTx moves away from the LTx when $\phi = \pi/3 \in \mathcal{A}$; on the other hand, when $\phi = \pi/18 \notin \mathcal{A}$, the capacity C_3 exhibits a local minimum at $d_{12}/d_{13} = d_{\min}(\pi/18) = 0.5252$ and a local maximum at $d_{12}/d_{13} = d_{\max}(\pi/18) = 0.9520$ (i.e., near the LRx). Similar conclusions can be drawn from the outage probability $P_{\text{out},3}$ given by (35), as reported in Figs. 5 and 6.

It is important to observe that even small values of ΔC_3 lead to significant increments in terms of data rate for the legacy transmission. For instance, it can be seen from results of Fig. 3 that, when $\phi = \pi/18$ and the BTx employs a QPSK modulation, one gets $\Delta C_3 = 0.1315$ b/s/Hz at $\mathbb{E}[|\Gamma(n)|^2] = -40$ dB. In this case, if the LTx is a TV tower broadcasting over a bandwidth of 6 MHz [3], then the data-rate gain is equal to 789 kbps; on the other hand, if the LTx is a Wi-Fi access point (AP) operating over a bandwidth of 20 MHz [4], [5], the gain is 2.63 Mbps.

B. Performance of the backscatter system when the LTx and BRx are co-located

Herein, we focus on the ergodic capacity C_1 of the backscatter system when the intended recipient BRx of the backscatter transmission is just the energy source LTx. More precisely, we report in Figs. 7

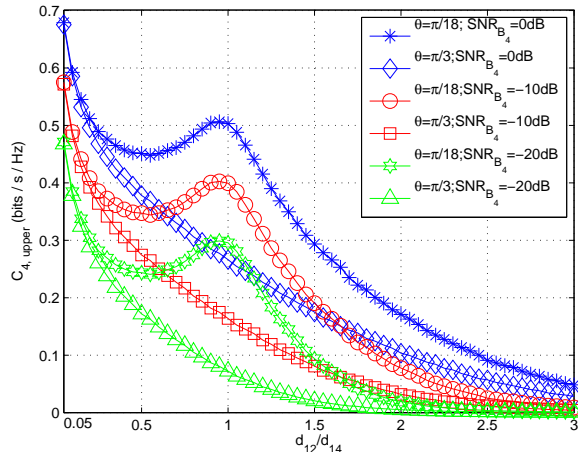


Figure 9. Best-case ergodic capacity of the backscatter system versus d_{12}/d_{14} for different values of $\text{SNR}_{B,4}$ (LTx and BRx are spatially-separated nodes).

and 8 its upper bound $C_{1,\text{upper}}$ given by (48) and lower bound $C_{1,\text{lower}}$ given by (53) for PSK modulations, respectively, as a function of d_{12}/d_{13} for different values of $\text{SNR}_{B,1}$. We also report in Fig. 8 the worst-case ergodic capacity of the backscatter system for the 4-ASK case, which is obtained by averaging (52) with respect to ψ .

As predicted by the performance analysis developed in Subsection V-A, both the upper and lower bounds are monotonically decreasing function of the distance between the LTx and the BTx, for each value of $\text{SNR}_{B,1}$. Moreover, when d_{12} is sufficiently smaller than d_{13} , it results that $C_{1,\text{lower}} \approx (\log Q)/M = 0.0625$, for each considered value of $\text{SNR}_{B,1}$. The slight performance advantage offered by the QPSK signal constellation over the 4-ASK one is due to the fact that the PSK modulation maximizes the cut-off rate in the case of equiprobable symbols (see Subsection V-A2). Results not reported here show that the gap between $C_{1,\text{upper}}$ and $C_{1,\text{lower}}$ is reduced for increasing values of Q .

Let us focus on the case when the LTx is a Wi-Fi AP transmitting over a bandwidth of 20 MHz, which might be used to connect the BTx to the Internet [4], [5]. In this scenario, by considering an indoor Wi-Fi network with $d_{13} = 100$ m, we obtain from Fig. 8 that the backscatter communication can achieve at least 1.25 Mbps up to a range of 50 – 70 m, even for very small values of $\text{SNR}_{B,1}$. As a comparison, we underline that the prototype presented in [5] is able to achieve communication rates up to 1 – 5 Mbps at a range of 1 – 5 m. Therefore, compared to [5], it is possible in theory to largely extend the communication range, without significantly reducing the data rate.

C. Performance of the backscatter system when the LTx and BRx are spatially-separated nodes

The last scenario under investigation is when the nodes LTx and BRx are distinct one from the other, with $\theta \in \{\pi/18, \pi/3\}$ and $d_{14} = 1$. Fig. 9 depicts the upper bound $C_{4,\text{upper}}$ given by (66) as a function of d_{12}/d_{14} ,

for different values of $\text{SNR}_{\text{B},4}$. Results corroborate the discussion reported in Remark 9, for each value of $\text{SNR}_{\text{B},4}$. In particular, if $\theta = \pi/3 \in \mathcal{A}$, then $C_{4,\text{upper}}$ monotonically decreases as the distance between the BTx and the LTx increases; when $\theta = \pi/18 \notin \mathcal{A}$, the capacity $C_{4,\text{upper}}$ assumes a global maximum when the BTx tends to be close by the LTx and a local maximum when the BTx is near the BRx, i.e., $d_{12}/d_{14} = d_{\text{max}}(\pi/18) = 0.9520$, by taking on a local minimum at $d_{12}/d_{14} = d_{\text{min}}(\pi/18) = 0.5252$.

In Fig. 10, the capacity $C_{4,\text{lower}}$ given by (72) is reported as a function of the $\text{SNR}_{\text{B},4}$ for different backscatter signal constellations, with $d_{12}/d_{14} = 0.2$, whereas $C_{4,\text{lower}}$ is reported in Fig. 11 as a function of d_{12}/d_{14} , with $\text{SNR}_{\text{B},4} = -20$ dB. It is seen that, also in this case, PSK constellations ensure better performance in terms of cut-off rate when the symbols are equiprobable. Another interesting conclusion that can be drawn from Fig. 10 is that all curves exhibit a capacity saturation effect, for vanishingly small noise, which is due to the interference generated by the legacy system over the $1 \rightarrow 4$ link. Moreover, independently of the considered backscatter signal constellation, the capacity $C_{4,\text{lower}}$ is a monomodal function of d_{12}/d_{14} having a maximum at $d_{12}/d_{14} \approx 0.3$ when $\theta = \pi/3 \in \mathcal{A}$, whereas, for $\theta = \pi/18 \notin \mathcal{A}$, it is multimodal by exhibiting slight fluctuations over a large interval of distances ranging from $d_{12}/d_{14} \approx 0.2$ to $d_{12}/d_{14} \approx 1.2$.

Let us consider the practical scenario when the LTx is a TV tower broadcasting over a bandwidth of 6 MHz [3], with $d_{14} = 4$ Km. In this case, according to the results of Fig. 10, by employing a QPSK backscatter signal constellation, the worst-case achievable data rate is equal to 360 kbps over a distance of 800 m at $\text{SNR}_{\text{B},4} = -10$ dB. As a comparison, we underline that the prototype presented in [3] is able to achieve information rates of 1 kbps over a distance of 5 – 8 m. Therefore, compared to [3], it is possible in theory to significantly extend both the communication range and the data rate.

VII. CONCLUSIONS

We developed a general framework for evaluating the ultimate achievable rates of a point-to-point backscatter communication network, by considering the influence of the backscatter transmission on the performance of the legacy system, from which energy is opportunistically harvested. Our theoretical results show that, in principle, ambient backscatter allows a passive device to achieve significant communication rates over short distances. As a by-product, the backscatter transmission can even ensure a performance improvement of the legacy system, provided that the latter one is designed to exploit the additional diversity arising from the backscatter process.

In view of the prototypes and experiments presented in [3], [4], [5], we highlight that there is plenty of scope for performance improvement, which mandates the use of advanced signal processing techniques, especially at the intended recipient of the backscatter information. Moreover, results of our performance

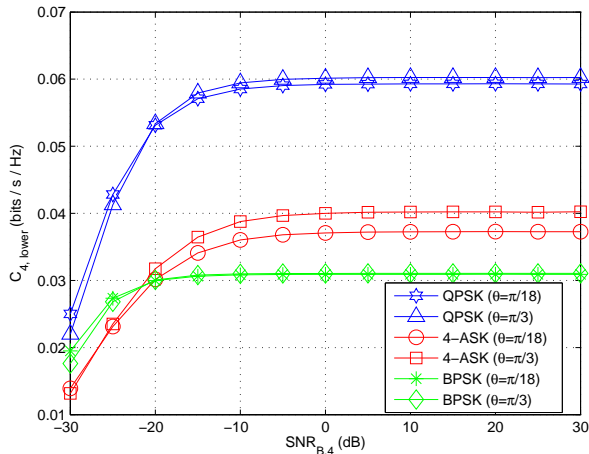


Figure 10. Worst-case ergodic capacity of the backscatter system versus $\text{SNR}_{B,4}$ for three backscatter signal constellations and two values of the angle ϕ (LTx and BRx are spatially-separated nodes).

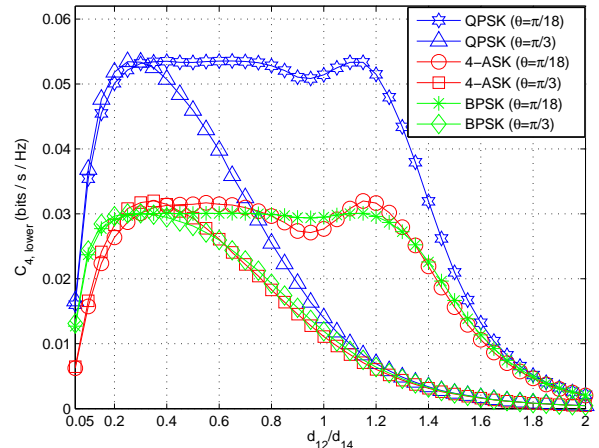


Figure 11. Worst-case ergodic capacity of the backscatter system versus d_{12}/d_{14} for two backscatter signal constellations and two values of the angle ϕ (LTx and BRx are spatially-separated nodes).

analysis pave the way towards various system-level optimizations. Among the others, an interesting issue is to analytically determine what is the optimal choice of $\mathbb{E}[|\Gamma(n)|^2]$ that ensures the best tradeoff between performance of legacy/backscatter systems and energy harvesting at the passive backscatter transmitter.

REFERENCES

- [1] C. Boyer and S. Roy, "Backscatter communication and RFID: Coding, Energy, and MIMO analysis", *IEEE Trans. Commun.*, pp. 770–785, Mar. 2014.
- [2] D. Darsena, G. Gelli, and F. Verde, "Exploiting noncircularity in backscattering communications", in *Proc. of the Twelfth International Symposium on Wireless Communication Systems (ISWCS)*, Brussels, Belgium, Aug. 2015, pp. 1-5.
- [3] V. Liu, A. Parks, V. Talla, S. Gollakota, D. Wetherall, and J.R. Smith, "Ambient backscatter: wireless communication out of thin air", in *Proc. of ACM SIGCOMM'13*, Hong Kong, China, Aug. 2013, pp. 39–50.
- [4] B. Kellogg, A. Parks, S. Gollakota, J.R. Smith, and D. Wetherall, "Wi-Fi backscatter: Internet connectivity for RF-powered devices", in *Proc. of ACM SIGCOMM'14*, Chicago, Illinois, USA, Aug. 2014, pp. 607–618.
- [5] D. Bharadia, K. Joshi, M. Kotaru, S. Katti, "BackFi: High throughput WiFi backscatter", in *Proc. of ACM SIGCOMM'15*, London, United Kingdom, Aug. 2015, pp. 283–296.
- [6] Z. Ma, T. Zeng, G. Wang, and F. Gao, "Signal detection for ambient backscatter system with multiple receiving antennas", in *Proc. of IEEE 14th Canadian Workshop on Information Theory (CWIT)*, St. John's, NL, Canada, July 2015, pp. 50-53.
- [7] K. Lu, G. Wang, F. Qu, and Z. Zhong, "Signal detection and BER analysis for RF-powered devices utilizing ambient backscatter", in *Proc. of International Conference on Wireless Communications & Signal Processing (WCSP)*, Nanjing, China, Oct. 2015, pp. 1-5.
- [8] G. Wang, F. Gao, Z. Dou, and C. Tellambura, "Uplink Detection and BER Analysis for Ambient Backscatter Communication Systems", in *Proc. of IEEE Global Communications Conference (Globecom)*, San Diego, CA, USA, Dec. 2015, pp. 1-6.
- [9] H. Shariatmadari *et al.*, "Machine-type communications: Current status and future perspectives toward 5G systems", *IEEE Commun. Magazine*, pp. 10–17, Sep. 2015.
- [10] A. Sabharwal *et al.*, "In-band full-duplex wireless: Challenges and opportunities," *IEEE J. Select. Areas Commun.*, vol. 32, pp. 1637–1652, Sep. 2014.
- [11] R. A. Horn and C. R. Johnson, *Matrix Analysis*, Cambridge: Cambridge University Press, 1990.
- [12] Z. Wang and G.B. Giannakis, "Wireless multicarrier communications – where Fourier meets Shannon," *IEEE Signal Processing Magazine*, pp. 29–48, May 2000.

- [13] H. Stockman, "Communication by means of reflected power", *Proc. IRE*, pp. 1196–1204, Oct. 1948.
- [14] S.J. Thomas, E. Wheeler, J. Teizer, and M.S. Reynolds, "Quadrature amplitude modulated backscatter in passive and semipassive UHF RFID systems", *IEEE Trans. Microw. Theory Tech.*, pp. 1175–1182, Apr. 2012.
- [15] D.D. King, "The measurement and interpretation of antenna scattering", *Proc. IRE*, pp. 770–777, July 1949.
- [16] K. Kurokawa, "Power waves and the scattering matrix", *IEEE Trans. Microw. Theory Tech.*, pp. 194–202, Mar. 1965.
- [17] D. Arnitz, U. Muehlmann, and K. Witrissal, "Tag-based sensing and positioning in passive UHF RFID: Tag reflection", in *Proc. of 3rd Int. EURASIP Workshop RFID Technol.*, Cartagena, Spain, Sep. 2010, pp. 51–56.
- [18] R.C. Hansen, "Relationships between antennas as scatters and radiators", *Proc. IEEE*, pp. 659–662, May 1969.
- [19] U. Mengali and A.N. D'Andrea, *Synchronization Techniques for Digital Receivers*, New York: Plenum, 1997.
- [20] M. Morelli, C.-C.J. Kuo, and M.-O. Pun, "Synchronization techniques for orthogonal frequency division multiple access (OFDMA): a tutorial review," *Proc. IEEE*, vol. 95, pp. 1394–1427, July 2007.
- [21] B. Picinbono, "On circularity," *IEEE Trans. Signal Process.*, vol. 42, pp. 3473–3482, Dec. 1994.
- [22] I.E. Telatar, "Capacity of multi-antenna Gaussian channels," *Eur. Trans. Telecommun.*, vol. 10, pp. 585–595, Nov./Dec. 1999.
- [23] R.G. Gallager, *Information Theory and Reliable Communication*, New York: Wiley, 1968.
- [24] T.M. Cover and J.A. Thomas, *Elements of Information Theory*, New York: Wiley, 1991.
- [25] E. Biglieri, J.G. Proakis, and S. Shamai, "Fading Channels: Information-Theoretic and Communications Aspects," *IEEE Trans. Inf. Theory*, vol. 44, pp. 2916–2692, Oct. 1998.
- [26] L. Ozarow, S. Shamai, and A. Wyner, "Information theoretic considerations for cellular mobile radio," *IEEE Trans. Veh. Technol.*, vol. 43, pp. 359 – 378, May 1994.
- [27] M. Morelli and U. Mengali, "A comparison of pilot-aided channel estimation methods for OFDM systems," *IEEE Trans. Signal Process.*, pp. 3065–3073, Dec. 2001.
- [28] J G. Smith, "The information capacity of amplitude and variance-constrained scalar Gaussian channels," *Inf. Contr.*, pp. 203–219, 1971.
- [29] F.D. Neeser and J.L. Massey, "Proper complex random processes with applications to information theory," *IEEE Trans. Inf. Theory*, pp. 1293–1302, July 1993.
- [30] Y. Wu and S. Verdú, "The impact of constellation cardinality on Gaussian channel capacity," in *Proc. of the 48th Annual Allerton Conference on Communication, Control, and Computing (Allerton)*, Allerton, IL, USA, Sep.-Oct. 2010, pp. 620–628.
- [31] A. Papoulis. *Probability, Random variables, and Stochastics Processes (3rd ed.)*. McGraw-Hill, Singapore, 1991.
- [32] S.G. Wilson. *Digital Modulation and Coding*. Englewood Cliffs, NJ: Prentice Hall, 1996.
- [33] T.L. Marzetta and B.M. Hochwald, "Capacity of a mobile multiple-antenna communication link in Rayleigh flat fading," *IEEE Trans. Inf. Theory*, vol. 45, pp. 139–157, Jan. 1999.
- [34] B.M. Hochwald and T.L. Marzetta, "Unitary space-time modulation for multiple-antenna communications in Rayleigh flat fading," *IEEE Trans. Inf. Theory*, vol. 46, pp. 543–564, Mar. 2000.
- [35] L. Zheng and D.N.C. Tse, "Communication on the Grassmann Manifold: A geometric approach to the noncoherent multiple-antenna channel," *IEEE Trans. Inf. Theory*, vol. 48, pp. 359–383, Feb. 2002.